MNRAS **000**, 1–?? (2018) Preprint December 14, 2018 Compiled using MNRAS LATEX style file v3.0

Reporting a Deficit of Intrinsic N V Absorbers in Core-dominated, Radio-loud Quasars

Chris Culliton[1⋆], Amber Roberts[1], Bryan DeMarcy[1], Sowgat Muzahid[1] Jane Charlton[1], Mike Eracleous[1], Rajib Ganguly[2], Jeffery Derseweh[2] Toru Misawa[3],

[1] *Dept. of Astronomy & Astrophysics, The Pennsylvania State University, 525 Davey Lab, University Park, PA 16802, USA*
[2] *Dept. of Comp. Sci., Engr., & Phys., University of Michigan-Flint, Murchie Science Building, 303 Kearsley Street, Flint, MI, 48502, USA*
[3] *School of Gen. Education, Shinshu University, 3-1-1 Asahi, Matsumoto, Nagano, 390-8621, Japan*

Accepted. Received; in original form

ABSTRACT

We searched ultraviolet spectra from the Hubble Space Telescope Cosmic Origins Spectrograph archive to locate intrinsic N V absorption systems. Our survey uncovered 59 intrinsic N V systems in the spectra of 428 low-redshift quasars, all found within the associated region ($|\Delta v| \leqslant 5000$ km s^{-1}). We consider the incidence of intrinsic absorbers as a function of quasar properties (optical, radio and X-ray). We find no intrinsic N V systems in the spectra of the radio-loud quasars, compared to 30% of the radio-quiet quasars containing at least one intrinsic system. Assuming intrinsic systems are equally likely to occur in radio-loud and radio-quiet quasars, there is a 0.5% probability of such a deficit occurring by chance in the radio-loud population. We propose that such a deficit of systems is caused by orientation effects: the available FIRST radio images show that 7 of the 10 radio-loud quasars have compact radio morphologies and a flat radio spectrum, implying that these quasars are face on, and that clouds that produce N V absorption are rarely found along the polar axis.

Key words: accretion, accretion discs – galaxies: active – quasars: absorption lines – quasars: general

1 INTRODUCTION

The absorbers found within quasar outflows are believed to be affected by the properties of the quasar. One important property of a quasar is its radio-loudness, which determines whether a quasar is radio-loud or radio-quiet. A current theory for this dichotomy is a modified version of the spin paradigm (Chiaberge & Marconi 2011) in which the radio-loudness of an AGN is determined not only by the spin, but also by the mass of the supermassive black hole (SMBH). Radio-loud quasars are believed to have SMBHs that are both rapidly spinning and massive ($M > 10^8$ M$_\odot$), while radio-quiet quasars having a rapidly spinning black hole with relatively low mass, or a non-spinning black hole of any size. An example of an effect of quasar radio properties on their outflows can be seen in Richards et al. (1999) and Richards (2001) where it was found that there were more C IV absorbers at velocity offsets over 5000 km s^{-1} in the spectra of radio-quiet quasars than there were in radio-loud quasars. These studies focused on medium- to high-redshift quasars. It should be noted that the effect of quasar properties on outflows could evolve with respect to redshift.

Quasar outflows can take the form of bipolar jets and/or accretion disk winds, and have been identified as an essential component of galaxy evolution. The feedback from the winds can impart momentum to the interstellar medium (ISM). This depletes the host galaxy of gas and dust, which disrupts star formation within the galaxy (Granato et al. 2004; Di Matteo et al. 2005; Springel et al. 2005; Ciotti & Ostriker 2007). The jets can also enrich the intergalactic medium (IGM) with heavy elements (Scannapieco & Oh 2004). To better understand the effects of the quasar outflows on galaxies, it is important to better understand the properties of the outflows.

Outflowing gas that originates with or is physically associated with the quasar is termed "intrinsic absorption." These outflowing absorbers are often observed through the rest frame UV transitions. They can be used to probe many properties of the outflows, including the kinematics, ionization state, and chemical composition of the gas. There are multiple categories of intrinsic absorbers, based upon the width of the absorption trough: broad absorption lines (BALs; width $>$ 2000 km s^{-1}), mini-BALs (widths 500 km s^{-1} $< v <$ 2000 km s^{-1}), and narrow absorption lines (NALs; widths $<$ 500 km s^{-1}). Both BALs and mini-BALs are believed to be intrinsic due to their exceedingly large width that could not be reproduced by intervening material along the line of sight to the quasar. At the small extreme, intrinsic NALs are almost indistinguishable from intervening absorbers, but can still be shown to be intrinsic in a variety of ways (Barlow et al. 1997).

Many previous studies have attempted to determine the

⋆ E-mail: csc189@psu.edu

rate of occurrence of intrinsic systems. Some of the first studies (Weymann et al. 1979; Foltz et al. 1986; Anderson et al. 1987) found that there was a statistical excess of C IV doublet lines within the associated region ($|v_{shift}| < 5000$ km s^{-1}) of radio-loud, steep-spectrum quasars over what would be expected if NALs were randomly distributed in space. It was assumed that such an excess was caused by intrinsic absorption. However, studies of radio-loud, flat-spectrum quasars found no such excess (Young et al. 1982; Sargent et al. 1988; Ganguly et al. 2001). Later studies attempted to determine properties of quasars that may make intrinsic absorption more or less likely. One such attempt (Ganguly et al. 2001) used a multivariate analysis of quasar properties, and discovered that radio-loud quasars with a flat radio spectrum and a weak C IV emission line did not contain intrinsic absorption in their spectra. Meanwhile, radio-quiet quasars that were soft X-ray weak were more likely to contain intrinsic absorption systems, including NALs, mini-BALs, and BALs. One possible explanation for this is that radio properties and inclination play a large role in determining whether or not intrinsic systems are found along a given quasar sightline. In this model, low inclination[1], radio-loud quasars are devoid of intrinsic absorbers along the poles, while the most dense gas, and hence most intrinsic absorption, occurs in radio-quiet quasars along the accretion disk. Intrinsic absorption was found in radio-loud quasars at high inclination angles, but not to the extent that it is found toward radio-quiet quasars, nor are BALs present toward radio-loud quasars. This implies that the density of the fast wind in radio-loud quasars is low enough that BALs do not often appear in their spectra.

Although the surveys listed above focused on C IV, in this paper we use N V NALs, as such NALs have been shown to have a higher intrinsic occurrence rate (e.g. Misawa et al. 2007; Culliton et al. 2018a) as compared to other ions, such as C IV or Si IV. N V NALs tend to have velocity structures indicative of an intrinsic system, and also have high ionization levels. Some can be shown to be intrinsic because of demonstrated partial covering of the quasar continuum source and/or broad emission line region (Misawa et al. 2007; Culliton et al. 2018a). Combined with the metal-rich environment around a quasar (Wu et al. 2010), these types of systems are very likely to be intrinsic.

In §2, we define the sample. In §3, we explain our method of surveying intrinsic N V systems. In §4, we describe the survey results and correlations found, and compare them to previous samples. Finally, we describe the implications for rate of incidence for intrinsic systems due to inclination angle in §5, and summarize the results in §6.

2 SAMPLE PROPERTIES

The Cosmic Origins Spectrograph (COS) was installed on the Hubble Space Telescope (HST) in May 2009. We obtained all publicly available spectra of redshift $z < 2$ quasars observed by COS between the time of installation and August 2015. The sample of 428 low-redshift quasars in which we searched for N V absorbers had the following selection criteria: (1) archived HST/COS observations obtained with either the G130M and/or the G160M echelle gratings, (2) spectra with signal-to-noise (S/N) ratio per resolution element $\geqslant$3, and (3) observations made prior to February 2015. The properties of COS and its in-flight operations are characterized by Osterman et al. (2011) and Green et al. (2012). We retrieved the flux-calibrated data from the HST archive and reduced it using the STScI CALCOS v.2.12 pipeline. The individual G130M and G160M grating integrations were combined together in flux units weighted by their respective exposure time using the the software developed by the COS GTO team[2]. A full description of this routine is given in Danforth et al. (2010). The procedures followed for data reduction are described in greater detail in Narayanan et al. (2011).

The COS instrument, with its G130M and G160M gratings, provides medium resolution ($R = 20,000$) spectra in a wavelength range of 1150−1750 Å, allowing us to search for N V $\lambda\lambda$1239, 1243 Å doublets at $z < 0.4$. Due to limitations of HST/COS resolution (it broadens lines, the LSF of the COS spectra is not Gaussian, components blend together, etc.), as well as the low signal-to-noise of some of the spectra, and contamination by blends affecting the N V doublets, a partial coverage analysis was not feasible.

Observational details of the quasars can be found in Table 1, which includes the original observer, the quasar emission redshift, the wavelengths covered, and the redshifts and velocities covered with respect to N V. Some of the quasars have gaps in their wavelength coverage. Therefore, each line in the table is a different wavelength range covered by COS for the given quasar, as well as the associated redshift and velocity range covered.

In order to determine if the host quasar properties affect both the incidence rate and properties of the intrinsic NALs, we list the properties for all of the quasars in Table 2. Table 2 lists the emission redshift, z_{em}, the optical luminosity, L_ν(4400 Å), the radio luminosity, L_ν(radio), where "radio" is the frequency of the observation, and the corresponding L_ν(5 GHz) observation[3]. The luminosities were derived from the optical flux f_ν(opt) and the radio flux f_ν(5 GHz) using the luminosity distance formula given in Eq. (24) of Hogg (1999). In a few cases where the 1.4 GHz luminosity was unavailable, we note the alternative frequency that was used as a proxy. In this paper, we use the current WMAP cosmological parameters of $H_0 = 71$ km s^{-1} Mpc^{-1}, $\Omega_M = 0.266$, $\Omega_k = 0$, and $\Omega_\Lambda = 0.734$.

To determine which quasars are radio-loud we use the radio-loudness parameter, $\mathcal{R}$, which is defined as $\mathcal{R} = f_\nu(5\ \mathrm{GHz})/f_\nu(4400\ \text{Å})$ (Kellermann et al. 1989, 1994). The criterion for radio-loudness adopted by Kellermann et al. (1989, 1994) is $\mathcal{R} \geqslant 10$. However, as we were not always able to obtain the flux at 4400 Å, we instead used a value for radio-loudness parameter of $\mathcal{R} = f_\nu(5\ \mathrm{GHz})/f_\nu(3000\ \text{Å})$. The criterion for radio-loudness was unchanged. Table 2 lists $\mathcal{R}$ for each quasar, as well as an indication of whether the quasar is radio-loud (RL) or radio-quiet (RQ). The opti-

[1] Here, inclination is measured with respect to the polar axis

[2] http://casa.colorado.edu/∼danforth/science/cos/costools.html

[3] As in Culliton et al. (2018a), the value of L_ν(5 GHz) was obtained from L_ν(radio), assuming a radio spectral index of $\alpha_r = 0.7$.

Table 1: Quasar Observations

QSO	z_{em}	COS Prop ID	PI Name	λ_{down} ()	λ_{up} ()	$z_{down,\ N\ V}$	$z_{up,\ N\ V}$	$v_{down,\ N\ V}$ (km s^{-1})	$v_{up,\ N\ V}$ (km s^{-1})
2E 4066	0.297	11484	Ghavamian	1150	1292	−0.0717	0.0429	96688	64345
				1309	1579	0.0566	0.275	60597	5223
				1600	1775	0.292	0.433	1262	−29757
Mrk 817	0.031455	11505	Noll	1135	1798	−0.0838	0.451	35359	−98588
PKS 0405−123	0.57259	11508	Noll	1132	1798	−0.0862	0.451	148451	23995
2MASSI J1118302+402553	0.154338	11519	Green	1132	1798	−0.0862	0.451	68814	−67474
Ton 580	0.289477	11519	Green	1134	1799	−0.0846	0.452	98883	−35459
Mrk 421	0.030021	11520	Green	1132	1784	−0.0862	0.44	35731	−96867
QSO B2005−489	0.071	11520	Green	1135	1785	−0.0838	0.441	46427	−86418
MCG+13−07−002	0.131	11520	Green	1134	1784	−0.0846	0.44	62480	−71052
[VV98] J043938.7−531131	0.243	11520	Green	1136	1785	−0.083	0.441	88477	−43969
QSO B1553+113	0.36	11520	Green	1132	1798	−0.0862	0.451	113305	−19468
SBSG 1123+594A	0.85142	11520	Green	1136	1785	−0.083	0.441	181679	73620
[VV2000] J044011.9−524818	1.053	11520	Green	1135	1785	−0.0838	0.441	200213	101917
[VV2000] J043650.8−525849	1.231	11520	Green	1132	1785	−0.0862	0.441	213658	123309
Ton 151	0.037789	11522	Green	...	...	...	...	...	...
Mrk 335	0.025785	11524	Green	1136	1784	−0.083	0.44	33468	−97972
Mrk 290	0.029577	11524	Green	1135	1784	−0.0838	0.44	34821	−96982
QSO B1011−040	0.058314	11524	Green	1132	1786	−0.0862	0.442	43711	−89835
Mrk 1513	0.062977	11524	Green	1132	1798	−0.0862	0.451	45000	−90462
QSO B2347−4342	2.885	11528	Green	1134	1433	−0.0846	0.157	268256	250966
2MASS J21545109−4414057	0.344	11541	Green	1132	1798	−0.0862	0.451	110250	−22998
[VV2000] J015513.2−450612	0.451	11541	Green	1134	1784	−0.0846	0.44	129098	2265
LB 2522	0.4778	11541	Green	1132	1783	−0.0862	0.439	133955	7918
HE 0226−4110	0.493368	11541	Green	1132	1781	−0.0862	0.438	136458	11392
Ton 1329	0.508346	11541	Green	1136	1786	−0.083	0.442	137987	13540
QSO B0238−1904	0.631	11541	Green	1068	1782	−0.138	0.438	168855	37462
7C 113710.40+660425.00	0.646	11541	Green	1134	1784	−0.0846	0.44	158158	39830
NGC 5253	0.001358	11579	Tripp	1132	1274	−0.0862	0.0284	27364	−7986
				1291	1433	0.0421	0.157	−11955	−42948
LBQS 0107−0232	0.728	11585	Crighton	1132	1798	−0.0862	0.451	168768	51775
QSO J0110−0218	0.956	11585	Crighton	1132	1798	−0.0862	0.451	192380	86891
LBQS 0107−0235	0.957039	11585	Crighton	1132	1798	−0.0862	0.451	192473	87036
6dFGS gJ115758.8−002221	0.260247	11598	Tumlinson	1132	1798	−0.0862	0.451	93189	−42054
SBSG 0924+606B	0.29589	11598	Tumlinson	1136	1785	−0.083	0.441	99736	−31677
PB 159	0.374873	11598	Tumlinson	1132	1798	−0.0862	0.451	116088	−16219
2MASSI J1220351+385316	0.376654	11598	Tumlinson	1132	1283	−0.0862	0.0357	116418	83094
				1291	1798	0.0421	0.451	81370	−15832
QSO J1233+4758	0.38223	11598	Tumlinson	1132	1798	−0.0862	0.451	117445	−14623
PB 8488	0.424787	11598	Tumlinson	1132	1274	−0.0862	0.0284	125048	94417
				1291	1798	0.0421	0.451	90822	−5543
QSO J1435+3604	0.429945	11598	Tumlinson	1132	1798	−0.0862	0.451	125942	−4460
QSO J1616+4154	0.441195	11598	Tumlinson	1132	1274	−0.0862	0.0284	127870	97498

Table 1: (continued)

QSO	z_{em}	COS Prop ID	PI Name	λ_{down} ()	λ_{up} ()	$z_{down,\ N\ V}$	$z_{up,\ N\ V}$	$v_{down,\ N\ V}$ (km s^{-1})	$v_{up,\ N\ V}$ (km s^{-1})
				1291	1798	0.0421	0.451	93929	−2111
2MASSI J0803592+433258	0.448706	11598	Tumlinson	1159	1310	−0.0644	0.0575	123329	91377
				1318	1798	0.0639	0.451	89718	−553
QSO J1009+0713	0.456524	11598	Tumlinson	1136	1785	−0.083	0.441	129595	3236
QSO J0910+1014	0.462765	11598	Tumlinson	1132	1798	−0.0862	0.451	131491	2342
QSO J0820+2334	0.470563	11598	Tumlinson	1136	1784	−0.083	0.44	131924	6279
QSO J1619+3342	0.471598	11598	Tumlinson	1132	1798	−0.0862	0.451	132944	4147
QSO J0925+4004	0.471681	11598	Tumlinson	1159	1310	−0.0644	0.0575	127222	95635
				1318	1798	0.0639	0.451	93992	4164
QSO J1550+4001	0.497235	11598	Tumlinson	1132	1798	−0.0862	0.451	137072	9322
QSO J1133+0327	0.524519	11598	Tumlinson	1136	1785	−0.083	0.441	140495	16897
QSO J0943+0531	0.564325	11598	Tumlinson	1136	1785	−0.083	0.441	146452	24586
QSO J0401−0540	0.570898	11598	Tumlinson	1132	1798	−0.0862	0.451	148207	23674
QSO J1241+5721	0.583471	11598	Tumlinson	1132	1798	−0.0862	0.451	150006	26047
QSO J0950+4831	0.589461	11598	Tumlinson	1132	1798	−0.0862	0.451	150853	27170
QSO J2257+1340	0.594555	11598	Tumlinson	1132	1798	−0.0862	0.451	151568	28122
QSO J0226+0015	0.615648	11598	Tumlinson	1150	1798	−0.0717	0.451	150979	32022
QSO J1112+3539	0.635972	11598	Tumlinson	1150	1798	−0.0717	0.451	153759	35721
4C 02.27	0.649117	11598	Tumlinson	1132	1798	−0.0862	0.451	158948	38084
[VV2006] J151428.6+361958	0.695179	11598	Tumlinson	1132	1798	−0.0862	0.451	164798	46179
QSO J1445+3428	0.697233	11598	Tumlinson	1132	1274	−0.0862	0.0284	165051	138774
				1291	1798	0.0421	0.451	135633	46534
QSO J1245+3356	0.711698	11598	Green	1132	1798	−0.0862	0.451	166816	49013
QSO J1555+3628	0.714085	11598	Tumlinson	1132	1798	−0.0862	0.451	167104	49420
QSO J1553+3548	0.722987	11598	Tumlinson	1132	1798	−0.0862	0.451	168172	50929
QSO J0914+2823	0.735438	11598	Tumlinson	1136	1785	−0.083	0.441	168925	55128
2MASS J14372609+5045556	0.78226	11598	Tumlinson	1132	1798	−0.0862	0.451	174989	60716
PB 5524	0.79005	11598	Tumlinson	1159	1310	−0.0644	0.0575	171149	144682
				1318	1798	0.0639	0.451	143278	61969
LBQS 1019+0147	0.790321	11598	Tumlinson	1136	1785	−0.083	0.441	175183	64092
QSO J1016+4706	0.822222	11598	Tumlinson	1068	1798	−0.138	0.451	190132	67062
PB 2049	0.874715	11598	Tumlinson	1132	1798	−0.0862	0.451	184690	75097
2MASS J00362300+4316402	0.12	11632	Rich	1136	1274	−0.083	0.0284	59165	25519
				1290	1558	0.0413	0.258	21800	−34595
				1578	1735	0.274	0.401	−38363	−65915
2MASX J01013113+4229356	0.19	11632	Rich	1134	1276	−0.0846	0.03	76898	42987
				1290	1559	0.0413	0.258	39778	−16750
				1577	1750	0.273	0.413	−20179	−50917
QSO J1503−4152	0.335	11659	Winkler	...	...	...	...	...	...
[VV2006] J150255.2−415430	1.026	11659	Winkler	1168	1310	−0.0572	0.0575	193058	171422
				1327	1469	0.0712	0.186	168801	146803
Ton 153	1.014695	11667	Churchill	1405	1579	0.134	0.275	155509	128407
				1600	1775	0.292	0.433	125154	98397
2MAXI J0808+757	0.1	11686	Arav	1132	1798	−0.0862	0.451	54978	−81039

Table 1: (continued)

QSO	z_{em}	COS Prop ID	PI Name	λ_{down} ()	λ_{up} ()	$z_{down,\ N\ V}$	$z_{up,\ N\ V}$	$v_{down,\ N\ V}$ (km s^{-1})	$v_{up,\ N\ V}$ (km s^{-1})
SWIFT J2248.7−5109	0.1	11686	Arav	1132	1798	−0.0862	0.451	54978	−81039
LB 1727	0.104	11686	Arav	1132	1798	−0.0862	0.451	56029	−80029
2MASS J12305003+0115226	0.117	11686	Arav	1132	1798	−0.0862	0.451	59408	−76760
Mrk 876	0.129	11686	Arav	1132	1274	−0.0862	0.0284	62479	27899
				1288	1781	0.0397	0.438	24648	−71076
2MASX J00481899+3941118	0.134	11686	Arav	1132	1798	−0.0862	0.451	63745	−72512
6dFGS gJ050304.0−663346	0.064	11692	Howk	1132	1283	−0.0862	0.0357	45282	8091
				1291	1568	0.0421	0.266	6228	−51529
				1577	1764	0.273	0.424	−53192	−84965
2MASX J04382919−6147587	0.069	11692	Howk	1132	1283	−0.0862	0.0357	46655	9495
				1291	1568	0.0421	0.266	7633	−50164
				1577	1764	0.273	0.424	−51830	−83671
[VV98] J062309.1−643624	0.128889	11692	Howk	1132	1283	−0.0862	0.0357	62451	25776
				1290	1568	0.0413	0.266	24156	−34149
				1577	1764	0.273	0.424	−35842	−68384
QSO B0558−5026	0.1372	11692	Howk	1134	1274	−0.0846	0.0284	64046	30048
				1290	1558	0.0413	0.258	26340	−30080
				1578	1734	0.274	0.4	−33860	−61387
QSO J0635−7516	0.653	11692	Howk	1134	1274	−0.0846	0.0284	159074	132479
				1290	1558	0.0413	0.258	129451	79966
				1578	1734	0.274	0.4	76402	49407
2MASS J05522451−6402108	0.68	11692	Howk	1134	1274	−0.0846	0.0284	162534	136359
				1290	1558	0.0413	0.258	133375	84458
				1578	1734	0.274	0.4	80925	54119
LBQS 1218+1611	0.229453	11698	Putman	1141	1283	−0.079	0.0357	84257	50924
				1300	1442	0.0494	0.164	47084	16382
RMB 219	0.276924	11698	Putman	1141	1283	−0.079	0.0357	94603	61879
				1300	1442	0.0494	0.164	58090	27677
2MASS J12201843+0641196	0.286705	11698	Putman	1141	1283	−0.079	0.0357	96658	64065
				1300	1442	0.0494	0.164	60289	29943
LBQS 1214+0826	0.343511	11698	Putman	1141	1283	−0.079	0.0357	108096	76305
				1300	1442	0.0494	0.164	72602	42702
LBQS 1206+1052	0.395549	11698	Putman	1141	1283	−0.079	0.0357	117869	86852
				1300	1442	0.0494	0.164	83223	53799
RMB 145	0.411797	11698	Putman	1141	1283	−0.079	0.0357	120789	90020
				1300	1442	0.0494	0.164	86416	57150
LBQS 1222+0901	0.535225	11698	Putman	1141	1283	−0.079	0.0357	141104	112269
				1300	1442	0.0494	0.164	108860	80928
RMB 221	0.542691	11698	Putman	1141	1283	−0.079	0.0357	142233	113518
				1300	1442	0.0494	0.164	110120	82275
LBQS 1211+0841	0.586024	11698	Putman	1141	1283	−0.079	0.0357	148584	120556
				1300	1442	0.0494	0.164	117231	89894
2MASS J12164057+0712244	0.587563	11698	Putman	1141	1283	−0.079	0.0357	148803	120800
				1300	1442	0.0494	0.164	117477	90159
LBQS 1220+0939	0.682359	11698	Putman	1141	1283	−0.079	0.0357	161526	135016

Table 1: (continued)

QSO	$z_{\rm em}$	COS Prop ID	PI Name	$\lambda_{\rm down}$ ()	$\lambda_{\rm up}$ ()	$z_{\rm down,\ N\ V}$	$z_{\rm up,\ N\ V}$	$v_{\rm down,\ N\ V}$ (km s^{-1})	$v_{\rm up,\ N\ V}$ (km s^{-1})
				1300	1442	0.0494	0.164	131851	105685
2MASS J12342679+0724116	0.844509	11698	Putman	1141	1283	−0.079	0.0357	180129	156074
				1300	1442	0.0494	0.164	153178	129020
LBQS 1238+1006	1.046235	11698	Putman	...	...	...	...	...	...
4C 10.34	1.088576	11698	Putman	1141	1283	−0.079	0.0357	202175	181459
				1300	1442	0.0494	0.164	178939	157694
QSO J1236+0600	1.287934	11698	Putman	1141	1283	−0.079	0.0357	216176	197828
				1300	1442	0.0494	0.164	195581	176508
LEDA 27453	0.102119	11727	Heckman	1134	1279	−0.0846	0.0324	55024	19554
				1288	1587	0.0397	0.281	17459	−44767
				1599	1758	0.291	0.419	−46972	−74208
2MASS J21035875−0728025	0.136901	11727	Heckman	1168	1310	−0.0572	0.0575	55467	21679
				1327	1602	0.0712	0.293	17830	−38397
				1623	1798	0.31	0.451	−42231	−71790
LEDA 2816291	0.146965	11727	Heckman	1172	1317	−0.0539	0.0631	57027	22718
				1328	1610	0.072	0.3	20237	−37267
				1623	1796	0.31	0.45	−39638	−68979
LBQS 0052−0038	0.167606	11727	Heckman	1132	1278	−0.0862	0.0316	72051	36932
				1288	1433	0.0397	0.157	34628	2802
[SFL2007] 2	0.219161	11727	Heckman	1153	1297	−0.0693	0.047	79020	45300
				1308	1563	0.0558	0.262	42822	−10274
				1576	1752	0.272	0.414	−12754	−44176
2MASS J09215939+4509126	0.234794	11727	Heckman	1168	1310	−0.0572	0.0575	78969	46110
				1327	1568	0.0712	0.266	42329	−7414
				1589	1764	0.283	0.424	−11399	−42439
QSO J1617+0638	0.229454	11728	Heckman	1132	1798	−0.0862	0.451	86439	−49297
QSO B0748+295	0.915726	11741	Tripp	1151	1775	−0.0709	0.433	185617	84708
QSO J1409+2618	0.94	11741	Tripp	1151	1775	−0.0709	0.433	187926	88169
LB 2126	0.975979	11741	Tripp	1151	1775	−0.0709	0.433	191232	93174
QSO J1208+4540	1.164941	11741	Tripp	1151	1775	−0.0709	0.433	206537	117161
QSO J1341+4123	1.217076	11741	Tripp	1150	1798	−0.0717	0.451	210356	119923
LBQS 1435−0134	1.31079	11741	Tripp	1150	1798	−0.0717	0.451	216476	130173
QSO B1521+1009	1.328005	11741	Tripp	1150	1798	−0.0717	0.451	217535	131973
4C −04.06	1.437368	11741	Tripp	1151	1775	−0.0709	0.433	223721	145806
QSO B1630+3744	1.478949	11741	Tripp	1151	1798	−0.0709	0.451	225940	146730
NGC 4051	0.002336	11834	Turner	1134	1758	−0.0846	0.419	27129	−100226
NGC 3227	0.003859	11837	Elvis	1150	1786	−0.0717	0.442	23411	−104012
Mrk 509	0.034397	12022	Kaastra	1152	1752	−0.0701	0.414	31802	−90826
QSO B1048+342	0.167008	12024	Green	1132	1798	−0.0862	0.451	71906	−64359
2MASSI J1124392+420144	0.225	12024	Green	1132	1798	−0.0862	0.451	85441	−50355
[VV2000] J103216.1+505120	0.17314	12025	Green	1132	1798	−0.0862	0.451	73385	−62859
2FHL J1104.0−2331	0.186	12025	Green	1132	1798	−0.0862	0.451	76449	−59727
Ton 488	0.256429	12025	Green	1132	1798	−0.0862	0.451	92367	−42945
7C 071610.69+712601.00	0.3	12025	Green	1132	1798	−0.0862	0.451	101517	−32889

Table 1: (continued)

QSO	$z_{\rm em}$	COS Prop ID	PI Name	$\lambda_{\rm down}$ ()	$\lambda_{\rm up}$ ()	$z_{\rm down,\ N\ V}$	$z_{\rm up,\ N\ V}$	$v_{\rm down,\ N\ V}$ (km s^{-1})	$v_{\rm up,\ N\ V}$ (km s^{-1})
QSO B0832+2510	0.329684	12025	Green	1132	1798	−0.0862	0.451	107463	−26187
QSO B1028+511	0.360403	12025	Green	1132	1798	−0.0862	0.451	113381	−19380
[VV96] J111132.1+554725	0.768267	12025	Green	1132	1798	−0.0862	0.451	173424	58447
NAME MR 2251−178	0.06398	12029	Green	1132	1798	−0.0862	0.451	45277	−90205
Mrk 106	0.123366	12029	Green	1132	1798	−0.0862	0.451	61043	−75165
QSO B1626+5529	0.133	12029	Green	1132	1798	−0.0862	0.451	63493	−72761
LBQS 0302−0019	3.297184	12033	Green	1132	1460	−0.0862	0.179	273854	257848
QSO B2155−304	0.116	12038	Green	1132	1579	−0.0862	0.275	59150	−39604
				1600	1775	0.292	0.433	−43489	−73394
3C 273	0.158	12038	Green	1132	1460	−0.0862	0.179	69712	−5270
Ton 1388	0.176	12038	Green	...	...	...	...	...	...
QSO J2155−0922	0.19	12038	Green	1132	1798	−0.0862	0.451	77392	−58757
2XMM J095652.4+411522	0.2341	12038	Green	1132	1798	−0.0862	0.451	87475	−48196
ICRF J130533.0−103319	0.2784	12038	Green	1132	1798	−0.0862	0.451	97045	−37842
Ton 28	0.327201	12038	Green	1132	1798	−0.0862	0.451	106974	−26743
Ton 236	0.45	12038	Green	1132	1798	−0.0862	0.451	129360	−285
2E 12	0.4509	12038	Green	...	...	...	...	...	...
2MASS J02015718−1132334	0.670527	12038	Green	1132	1798	−0.0862	0.451	161709	41882
[VV2000] J102734.2+183428	2.84	12178	Anderson	1068	1208	−0.138	−0.0249	271021	263471
				1223	1364	−0.0128	0.101	262619	254243
[VV2010c] J104843.5+130605	0.218529	12198	Rosenberg	1141	1283	−0.079	0.0357	81787	48322
				1300	1568	0.0494	0.266	44471	−11386
				1589	1764	0.283	0.424	−15366	−46327
2MASS J10481625+1207344	0.29113	12198	Rosenberg	1141	1283	−0.079	0.0357	97579	65047
				1300	1442	0.0494	0.164	61276	30962
SDSS J104709.83+130454.6	0.400607	12198	Rosenberg	1141	1283	−0.079	0.0357	118785	87845
				1300	1442	0.0494	0.164	84223	54848
Ton S 210	0.116	12204	Thom	1132	1798	−0.0862	0.451	59150	−77010
2E 357	0.348858	12204	Thom	1132	1798	−0.0862	0.451	111184	−21923
QSO B0120−28	0.436018	12204	Thom	1132	1798	−0.0862	0.451	126986	−3190
NGC 4395	0.001064	12212	Crenshaw	1132	1798	−0.0862	0.451	27277	−106504
NGC 3516	0.008836	12212	Crenshaw	1132	1798	−0.0862	0.451	29574	−104473
NGC 7469	0.016317	12212	Crenshaw	1132	1798	−0.0862	0.451	31766	−102522
Mrk 1044	0.016451	12212	Crenshaw	1132	1798	−0.0862	0.451	31805	−102487
NGC 5548	0.017175	12212	Crenshaw	1132	1798	−0.0862	0.451	32016	−102299
UGC 12163	0.024684	12212	Crenshaw	1132	1798	−0.0862	0.451	34194	−100346
Mrk 279	0.030451	12212	Crenshaw	1132	1798	−0.0862	0.451	35854	−98849
NGC 3783	0.00973	12212/13115	Crenshaw	1132	1798	−0.0862	0.451	29837	−104240
NGC 4151	0.003319	12248	Tumlinson	1132	1798	−0.0862	0.451	27946	−105915
2MASX J14510879+2709272	0.065	12248	Tumlinson	1132	1798	−0.0862	0.451	45557	−89943
6dFGS gJ031027.9−004951	0.080139	12248	Tumlinson	1132	1798	−0.0862	0.451	49682	−86077
2MASS J15213967+0337292	0.1265	12248	Tumlinson	1132	1568	−0.0862	0.266	61843	−34776
				1577	1764	0.273	0.424	−36468	−68986
2MASX J09473320+1005093	0.13954	12248	Tumlinson	1132	1798	−0.0862	0.451	65139	−71135

Table 1: (continued)

QSO	z_{em}	COS Prop ID	PI Name	λ_{down} ()	λ_{up} ()	$z_{down,\ N\ V}$	$z_{up,\ N\ V}$	$v_{down,\ N\ V}$ (km s^{-1})	$v_{up,\ N\ V}$ (km s^{-1})
2MASS J13571260+1704439	0.1505	12248	Tumlinson	1132	1798	−0.0862	0.451	67867	−68421
2MASS J11211423+0325466	0.151994	12248	Tumlinson	1132	1798	−0.0862	0.451	68236	−68052
2MASS J09591566+0503552	0.162631	12248	Tumlinson	1150	1775	−0.0717	0.433	66361	−61747
[VV98] J135625.5+251524	0.164009	12248	Tumlinson	1132	1568	−0.0862	0.266	71178	−25055
				1577	1764	0.273	0.424	−26758	−59619
6dFGS gJ015530.0−085704	0.164427	12248	Tumlinson	1132	1798	−0.0862	0.451	71280	−64992
2E 2584	0.1653	12248	Tumlinson	1150	1775	−0.0717	0.433	67015	−61088
2MASS J12111454+3657395	0.171084	12248	Tumlinson	1132	1798	−0.0862	0.451	72890	−63361
2MASS J13423123+3829032	0.171894	12248	Tumlinson	1132	1798	−0.0862	0.451	73085	−63163
2MASS J02121832−0737198	0.17392	12248	Tumlinson	1132	1798	−0.0862	0.451	73572	−62668
2XMMi J123604.0+264135	0.209152	12248	Tumlinson	1159	1310	−0.0644	0.0575	75260	39949
				1318	1775	0.0639	0.433	38155	−50398
QSO J0012−1022	0.228191	12248	Tumlinson	1382	1798	0.116	0.451	28743	−49597
2MASS J09462126+4711312	0.230217	12248	Tumlinson	1132	1798	−0.0862	0.451	86610	−49116
[VV2006] J092909.9+464424	0.239981	12248	Tumlinson	1132	1602	−0.0862	0.293	88777	−12583
				1611	1798	0.3	0.451	−14259	−46807
2E 3076	0.24232	12248	Tumlinson	1132	1568	−0.0862	0.266	89292	−5594
				1577	1764	0.273	0.424	−7309	−40653
2E 3124	0.263917	12248	Tumlinson	1132	1798	−0.0862	0.451	93976	−41199
2MASS J09123540+2957252	0.305578	12248	Tumlinson	1132	1798	−0.0862	0.451	102652	−31621
[VV2000] J082633.5+074248	0.310655	12248	Tumlinson	1150	1775	−0.0717	0.433	99491	−26645
2MASS J12072101+2624292	0.322492	12248	Tumlinson	1150	1775	−0.0717	0.433	101883	−23969
[VV2006] J092554.5+453544	0.329891	12248	Tumlinson	1132	1798	−0.0862	0.451	107504	−26141
[VV2000] J132704.1+443504	0.330398	12248	Tumlinson	1150	1775	−0.0717	0.433	103460	−22193
PG 1049−005	0.3599	12248	Tumlinson	1132	1775	−0.0862	0.433	113286	−15644
QSO B0946+3916	0.366193	12248	Tumlinson	1132	1798	−0.0862	0.451	114470	−18111
QSO J0242−0759	0.377782	12248	Tumlinson	1132	1798	−0.0862	0.451	116626	−15587
PB 4055	0.3832	12248	Tumlinson	1132	1798	−0.0862	0.451	117623	−14413
2E 1208.0+3213	0.389374	12248	Tumlinson	1132	1798	−0.0862	0.451	118751	−13081
[VV2006] J110313.0+414154	0.403095	12248	Tumlinson	1132	1798	−0.0862	0.451	121225	−10139
Ton 576	0.422294	12248	Tumlinson	1132	1775	−0.0862	0.433	124614	−2209
Ton 52	0.435718	12248	Tumlinson	1150	1775	−0.0717	0.433	123028	607
LB 2845	0.535312	12248	Tumlinson	1132	1798	−0.0862	0.451	142958	16836
QSO J1059+1441	0.63171	12248	Tumlinson	1132	1798	−0.0862	0.451	156648	34950
[VV2006] J080908.1+461925	0.658724	12248	Tumlinson	1132	1798	−0.0862	0.451	160196	39796
2MASS J10595880+2517089	0.662779	12248	Tumlinson	1132	1602	−0.0862	0.293	160718	73818
				1611	1798	0.3	0.451	72239	40515
2MASS J15455347+0936205	0.665	12248	Tumlinson	1150	1775	−0.0717	0.433	157609	44689
2MASS J11345760+2555279	0.709937	12248	Tumlinson	1132	1568	−0.0862	0.266	166603	87557
				1577	1764	0.273	0.424	85985	54267
QSO J1001+5944	0.747492	12248	Tumlinson	1132	1798	−0.0862	0.451	171050	55031
QSO J1122+5755	0.90685	12248	Tumlinson	1132	1798	−0.0862	0.451	187819	79852
[VV2006] J084349.5+411741	0.990788	12248	Tumlinson	1132	1798	−0.0862	0.451	195453	91706
4C 06.41	1.27	12252	Churchill	1394	1568	0.125	0.266	181520	157591

Table 1: (continued)

QSO	z_{em}	COS Prop ID	PI Name	λ_{down} ()	λ_{up} ()	$z_{down,\ N\ V}$	$z_{up,\ N\ V}$	$v_{down,\ N\ V}$ (km s^{-1})	$v_{up,\ N\ V}$ (km s^{-1})
				1589	1764	0.283	0.424	154685	130485
2E 1185	0.533739	12252/12466	Churchill/Charlton	1382	1568	0.116	0.266	92337	56883
				1577	1764	0.273	0.424	55227	22229
ESO 31−8	0.027619	12263	Misawa	1132	1274	−0.0862	0.0284	35040	−227
				1291	1579	0.0421	0.275	−4201	−63591
				1600	1775	0.292	0.433	−67363	−96135
2MASX J02430962−7216476	0.1018	12263	Misawa	1132	1274	−0.0862	0.0284	55451	20636
				1291	1579	0.0421	0.275	16678	−43369
				1600	1775	0.292	0.433	−47240	−76991
ICRF J020213.6−762003	0.38939	12263	Misawa	1132	1775	−0.0862	0.433	118754	−9223
[VV2000] J100535.2+013444	1.0809	12264	Morris	1132	1798	−0.0862	0.451	202865	103568
[VV2006] J020930.8−043827	1.128	12264	Morris	1132	1798	−0.0862	0.451	206448	109431
QSO B1354+0450	1.234529	12264	Morris	1132	1798	−0.0862	0.451	213891	121892
ESO 267−13	0.01488	12275	Wakker	1132	1469	−0.0862	0.186	31347	−46290
Mrk 595	0.026982	12275	Wakker	1132	1469	−0.0862	0.186	34857	−42815
Mrk 504	0.035888	12275	Wakker	1132	1469	−0.0862	0.186	37408	−40276
2MASX J18324966+5340219	0.039	12275	Wakker	1132	1469	−0.0862	0.186	38293	−39392
FRL 303	0.040008	12275	Wakker	1168	1310	−0.0572	0.0575	29314	−4988
				1327	1469	0.0712	0.186	−8851	−39107
2MASX J01414319+1340328	0.045	12275	Wakker	1132	1469	−0.0862	0.186	39990	−37695
2dFGRS TGN305Z073	0.046399	12275	Wakker	1132	1469	−0.0862	0.186	40384	−37300
ESO 265−23	0.056576	12275	Wakker	1168	1310	−0.0572	0.0575	34000	−250
				1327	1469	0.0712	0.186	−4115	−34440
4C 10.08	0.07	12275	Wakker	1132	1469	−0.0862	0.186	46928	−30700
Ton 1187	0.079097	12275	Wakker	1168	1310	−0.0572	0.0575	40225	6072
				1327	1469	0.0712	0.186	2208	−28186
2MASX J09563012−0453174	0.1571	12275	Wakker	1132	1469	−0.0862	0.186	69492	−7345
QSO B1112+4306	0.301321	12275	Wakker	1132	1469	−0.0862	0.186	101787	27788
CTS 10	0.355503	12275	Wakker	1132	1469	−0.0862	0.186	112453	39860
[VV98] J071436.2+740811	0.371	12275	Wakker	1132	1469	−0.0862	0.186	115369	43203
QSO B0713+745	0.475	12275	Wakker	1132	1469	−0.0862	0.186	133500	64406
[VV96] J120158.8−135459	0.506	12275	Wakker	1132	1469	−0.0862	0.186	138452	70327
NAME Crt A	0.556458	12275	Wakker	1132	1469	−0.0862	0.186	146106	79588
2E 177	0.62326	12275	Wakker	1168	1310	−0.0572	0.0575	148543	121154
				1327	1469	0.0712	0.186	117903	91162
LEDA 3096550	0.0266	12276	Wakker	1132	1469	−0.0862	0.186	34747	−42924
UGC 10832	0.028341	12276	Wakker	1132	1469	−0.0862	0.186	35248	−42426
NGC 6387	0.02835	12276	Wakker	1132	1469	−0.0862	0.186	35251	−42424
MCG+11−19−030	0.030097	12276	Wakker	1132	1785	−0.0862	0.441	35752	−96997
Mrk 486	0.038934	12276	Wakker	1132	1469	−0.0862	0.186	38274	−39411
2MASX J15085291+6814074	0.058637	12276	Wakker	1132	1469	−0.0862	0.186	43801	−33863
2MASX J16252653+5727278	0.067	12276	Wakker	1132	1469	−0.0862	0.186	46107	−31532
MCG+10−22−028	0.073424	12276	Wakker	1132	1469	−0.0862	0.186	47862	−29752
2MASX J17032892+6141102	0.077319	12276	Wakker	1132	1469	−0.0862	0.186	48919	−28676

Table 1: (continued)

QSO	z_{em}	COS Prop ID	PI Name	λ_{down} ()	λ_{up} ()	$z_{down,\ N\ V}$	$z_{up,\ N\ V}$	$v_{down,\ N\ V}$ (km s^{-1})	$v_{up,\ N\ V}$ (km s^{-1})
2MASX J15192168+5908239	0.0781	12276	Wakker	1132	1469	−0.0862	0.186	49131	−28461
2MASSI J1529074+561606	0.099	12276	Wakker	1132	1469	−0.0862	0.186	54714	−22747
2MASX J15031625+6810067	0.114	12276	Wakker	1132	1469	−0.0862	0.186	58633	−18702
[VV98] J160820.5+601828	0.178	12276	Wakker	1132	1469	−0.0862	0.186	74549	−1980
7C 152258.39+634859.00	0.204	12276	Wakker	1132	1469	−0.0862	0.186	80655	4565
2MASSI J1521537+594019	0.2862	12276	Wakker	1132	1469	−0.0862	0.186	98674	24311
[VV2006] J171738.0+655939	0.292656	12276	Wakker	1132	1469	−0.0862	0.186	100011	25801
2MASS J14594959+5319091	0.338	12276	Wakker	1132	1469	−0.0862	0.186	109088	36026
2MASS J15272866+6548102	0.345	12276	Wakker	1132	1469	−0.0862	0.186	110443	37567
[VV98] J150455.5+564920	0.358894	12276	Wakker	1132	1469	−0.0862	0.186	113096	40596
[VV96] J155232.5+570515	0.366	12276	Wakker	1132	1469	−0.0862	0.186	114434	42129
2MASS J15003066+5517092	0.405336	12276	Wakker	1132	1469	−0.0862	0.186	121625	50437
QSO J1244+1721	1.28161	12466	Charlton	1405	1579	0.134	0.275	180995	157181
				1600	1775	0.292	0.433	154289	130214
LBQS 1230−0015	0.470945	12486	Bowen	1132	1798	−0.0862	0.451	132837	4014
6C 121837+460525	0.52539	12486	Bowen	1132	1469	−0.0862	0.186	141452	73940
SDSS J095109.12+330745.8	0.64477	12486	Bowen	1132	1469	−0.0862	0.186	158378	94729
QSO J1415+1634	0.74349	12486	Bowen	1141	1292	−0.079	0.0429	168973	141785
				1300	1451	0.0494	0.171	140345	113340
ICRF J145907.5+714019	0.904499	12486	Bowen	1132	1469	−0.0862	0.186	187594	132287
QSO J1407+5507	1.02694	12486	Bowen	1132	1469	−0.0862	0.186	198519	146909
2MASX J23390127+3621087	0.06448	12533	Martin	1168	1310	−0.0572	0.0575	36203	1984
				1327	1469	0.0712	0.186	−1881	−32233
6dFGS gJ010250.0−222157	0.117835	12533	Martin	1132	1274	−0.0862	0.0284	59623	24943
				1291	1433	0.0421	0.157	20992	−10254
2MASX J12022678−0129155	0.150694	12533	Martin	1150	1469	−0.0717	0.186	63413	−9008
2E 503	0.404	12536	Kulkarni	1168	1310	−0.0572	0.0575	113442	82774
				1327	1469	0.0712	0.186	79190	50160
QSO J0441−4313	0.59378	12536	Kulkarni	1132	1274	−0.0862	0.0284	151459	123537
				1291	1433	0.0421	0.157	120220	92923
SDSS J004042.10−110957.7	0.027405	12557	Gultekin	1428	1602	0.153	0.293	−34348	−67778
				1623	1798	0.31	0.451	−71471	−99639
3C 84	0.017559	12560	Johnstone	1405	1579	0.134	0.275	−32392	−66402
				1600	1775	0.292	0.433	−70157	−98773
Mrk 231	0.04217	12569	Veilleux	1150	1469	−0.0717	0.186	34533	−38495
Mrk 1298	0.06196	12569	Veilleux	1150	1469	−0.0717	0.186	40085	−32935
Mrk 771	0.06301	12569	Veilleux	1150	1469	−0.0717	0.186	40376	−32643
Ton 951	0.064	12569	Veilleux	1150	1469	−0.0717	0.186	40650	−32367
Mrk 478	0.079055	12569	Veilleux	1150	1469	−0.0717	0.186	44776	−28198
2XMM J135315.8+634546	0.0882	12569	Veilleux	1150	1469	−0.0717	0.186	47247	−25688
Mrk 1501	0.089338	12569	Veilleux	1150	1469	−0.0717	0.186	47552	−25377
2XMM J141348.3+440014	0.0896	12569	Veilleux	1150	1469	−0.0717	0.186	47623	−25305
Mrk 877	0.112438	12569	Veilleux	1132	1451	−0.0862	0.171	58228	−15437
2E 3305	0.126	12569	Veilleux	1132	1451	−0.0862	0.171	61716	−11812

Table 1: (continued)

QSO	z_{em}	COS Prop ID	PI Name	λ_{down} ()	λ_{up} ()	$z_{down,\ N\ V}$	$z_{up,\ N\ V}$	$v_{down,\ N\ V}$ (km s^{-1})	$v_{up,\ N\ V}$ (km s^{-1})
2E 93	0.142	12569	Veilleux	1132	1451	−0.0862	0.171	65754	−7587
2XMM J130946.9+081948	0.155	12569	Veilleux	1150	1469	−0.0717	0.186	64481	−7889
Mrk 1014	0.16311	12569	Veilleux	1150	1469	−0.0717	0.186	66479	−5793
4C 01.61	0.17374	12569	Veilleux	1150	1469	−0.0717	0.186	69067	−3066
Ton 1565	0.182923	12569	Veilleux	1132	1451	−0.0862	0.171	75720	2967
Ton 1057	0.192142	12569	Veilleux	1132	1451	−0.0862	0.171	77895	5293
2XMM J100726.0+124856	0.240613	12569	Veilleux	1132	1451	−0.0862	0.171	88916	17223
NGC 3259	0.005624	12577	Rest	1428	1602	0.153	0.293	−40671	−73843
				1623	1798	0.31	0.451	−77498	−105312
QSO J1323+343	0.44287	12593	Nestor	1394	1568	0.125	0.266	73035	39048
				1589	1764	0.283	0.424	35120	3960
7C 101940.79+394702.00	0.60365	12593	Nestor	1405	1579	0.134	0.275	99886	67662
				1600	1775	0.292	0.433	63892	33627
PB 9362	0.62546	12593	Nestor	1405	1579	0.134	0.275	103470	71494
				1600	1775	0.292	0.433	67747	37620
QSO J1400+553	0.84081	12593	Nestor	1405	1579	0.134	0.275	134818	105487
				1600	1775	0.292	0.433	102001	73584
[VV2000] J215647.3+224250	1.29	12593	Nestor	1405	1579	0.134	0.275	181693	157977
				1600	1775	0.292	0.433	155096	131105
QSO J1544+2743	0.16392	12603	Heckman	1150	1469	−0.0717	0.186	66677	−5584
QSO J1131+1556	0.18289	12603	Heckman	1141	1469	−0.079	0.186	73486	−738
A1 66	0.20059	12603	Heckman	1132	1469	−0.0862	0.186	79865	3715
2MASS J14294076+0321257	0.25309	12603	Heckman	1141	1469	−0.079	0.186	89487	16529
2MASS J15123716+0128461	0.26541	12603	Heckman	1150	1469	−0.0717	0.186	90013	19451
2MASS J15150742+0657082	0.2679	12603	Heckman	1141	1469	−0.079	0.186	92684	20038
2MASS J15020410+0645159	0.28775	12603	Heckman	1141	1469	−0.079	0.186	96876	24669
2MASS J13482237+2456498	0.29343	12603	Heckman	1132	1469	−0.0862	0.186	100170	25979
2MASS J08525922+0313207	0.29677	12603	Heckman	1132	1579	−0.0862	0.275	100856	5169
				1600	1775	0.292	0.433	1209	−29810
QSO J1033+2112	0.31523	12603	Heckman	1132	1469	−0.0862	0.186	104596	30945
QSO J0808+0514	0.36058	12603	Heckman	1132	1469	−0.0862	0.186	113414	40960
Ton 202	0.36413	12603	Heckman	1132	1469	−0.0862	0.186	114083	41727
QSO J1541+2817	0.37556	12603	Heckman	1132	1469	−0.0862	0.186	116215	44177
LB 10203	0.37898	12603	Heckman	1132	1556	−0.0862	0.256	116847	27915
				1577	1752	0.273	0.414	23926	−7569
2MASSI J0951239+354248	0.39842	12603	Heckman	1150	1469	−0.0717	0.186	116395	48999
2MASSI J1431258+244220	0.40659	12603	Heckman	1141	1469	−0.079	0.186	119860	50697
QSO J1509+0702	0.41786	12603	Heckman	1141	1469	−0.079	0.186	121864	53018
2E 2370	0.42199	12603	Heckman	1132	1469	−0.0862	0.186	124561	53862
2MASS J14065564+0157131	0.42657	12603	Heckman	1150	1469	−0.0717	0.186	121430	54794
QSO J1315+1525	0.44832	12603	Heckman	1132	1469	−0.0862	0.186	129077	59167
QSO J1454+3046	0.46527	12603	Heckman	1132	1469	−0.0862	0.186	131905	62511
QSO J1122+0318	0.47451	12603	Heckman	1150	1469	−0.0717	0.186	129601	64311
QSO J1142+3016	0.48139	12603	Heckman	1132	1568	−0.0862	0.266	134537	46784

Table 1: (continued)

QSO	$z_{\rm em}$	COS Prop ID	PI Name	$\lambda_{\rm down}$ ()	$\lambda_{\rm up}$ ()	$z_{\rm down,\ N\ V}$	$z_{\rm up,\ N\ V}$	$v_{\rm down,\ N\ V}$ (km s^{-1})	$v_{\rm up,\ N\ V}$ (km s^{-1})
				1577	1764	0.273	0.424	45108	11853
QSO J0930+2848	0.48678	12603	Heckman	1132	1469	−0.0862	0.186	135405	66677
QSO J0159+1345	0.50381	12603	Heckman	1141	1469	−0.079	0.186	136232	69914
QSO J0937+1700	0.50596	12603	Heckman	1150	1469	−0.0717	0.186	134698	70319
QSO J1155+2922	0.52012	12603	Heckman	1141	1469	−0.079	0.186	138785	72965
QSO J1325+2717	0.52209	12603	Heckman	1132	1469	−0.0862	0.186	140946	73330
QSO J1305+0357	0.54497	12603	Heckman	1141	1469	−0.079	0.186	142576	77519
QSO J1120+0413	0.54516	12603	Heckman	1150	1469	−0.0717	0.186	140775	77554
QSO J1404+3353	0.54912	12603	Heckman	1150	1469	−0.0717	0.186	141373	78269
QSO J0959+3203	0.56394	12603	Heckman	1150	1469	−0.0717	0.186	143582	80922
QSO J1115+0237	0.56651	12603	Heckman	1141	1469	−0.079	0.186	145767	81379
Ton 635	0.58943	12603	Heckman	1132	1469	−0.0862	0.186	150848	85396
QSO J0914+0837	0.64856	12603	Heckman	1141	1469	−0.079	0.186	157161	95350
QSO J1059+0519	0.75434	12603	Heckman	1141	1469	−0.079	0.186	170238	111763
QSO J0931+2628	0.7782	12603	Heckman	1132	1469	−0.0862	0.186	174537	115232
Ton 1009	0.80809	12603	Heckman	1150	1469	−0.0717	0.186	174714	119463
QSO J1002+3240	0.82881	12603	Heckman	1150	1469	−0.0717	0.186	176955	122324
QSO J1059+1211	0.99319	12603	Heckman	1141	1469	−0.079	0.186	194291	143052
9C J0936+3207	1.14975	12603	Heckman	1132	1469	−0.0862	0.186	208040	159919
QSO J1318+2628	1.23441	12603	Heckman	1141	1469	−0.079	0.186	212711	168032
QSO J1051+1247	1.28101	12603	Heckman	1141	1469	−0.079	0.186	215739	172227
QSO J1251+0554	1.37745	12603	Heckman	1150	1469	−0.0717	0.186	220473	180347
QSO B1115+080A	1.73502	12603	Heckman	1141	1283	−0.079	0.0357	238722	224600
				1300	1442	0.0494	0.164	222852	207844
[VV2006] J101256.1+045817	1.85537	12603	Heckman	1141	1283	−0.079	0.0357	243287	230084
				1300	1442	0.0494	0.164	228446	214350
QSO J1354+2430	1.87818	12603	Heckman	1132	1469	−0.0862	0.186	244891	212786
ESO 113−45	0.048175	12604	Fox	1132	1274	−0.0862	0.0284	40883	5710
				1291	1568	0.0421	0.266	1737	−55877
				1589	1764	0.283	0.424	−59717	−89079
2MASX J01002713−5113544	0.06282	12604	Fox	1132	1274	−0.0862	0.0284	44957	9867
				1291	1568	0.0421	0.266	5896	−51852
				1589	1764	0.283	0.424	−55712	−85271
Mrk 304	0.065762	12604	Fox	1132	1568	−0.0862	0.266	45767	−51047
				1589	1764	0.283	0.424	−54911	−84508
2MASS J00583738−3606048	0.16414	12604	Fox	1132	1274	−0.0862	0.0284	71210	36979
				1291	1568	0.0421	0.266	33060	−25022
				1589	1764	0.283	0.424	−28978	−59587
2MASS J22452029−4652116	0.198	12604	Fox	1132	1274	−0.0862	0.0284	79264	45412
				1291	1568	0.0421	0.266	41521	−16468
				1589	1764	0.283	0.424	−20441	−51286
GD 1332	0.2	12604	Fox	1132	1274	−0.0862	0.0284	79728	45900
				1291	1568	0.0421	0.266	42012	−15970
				1589	1764	0.283	0.424	−19944	−50800

Table 1: (continued)

QSO	z_{em}	COS Prop ID	PI Name	λ_{down} ()	λ_{up} ()	$z_{down,\ N\ V}$	$z_{up,\ N\ V}$	$v_{down,\ N\ V}$ (km s^{-1})	$v_{up,\ N\ V}$ (km s^{-1})
7C 1424+2401	0.16	12612	Stocke	1132	1798	−0.0862	0.451	70202	−66079
2MASS J15095219+1110469	0.28506	12614	Gnat	1132	1274	−0.0862	0.0284	98437	65711
				1291	1433	0.0421	0.157	61917	31421
[VV2006] J160519.8+144853	0.37206	12614	Gnat	1132	1274	−0.0862	0.0284	115566	84116
				1291	1433	0.0421	0.157	80441	50684
7C 160253.79+573900.00	2.85	12816	Syphers	1068	1208	−0.138	−0.0249	271163	263648
				1223	1364	−0.0128	0.101	262800	254461
[VV2000] J091510.0+475657	3.33686	12816	Syphers	1068	1208	−0.138	−0.0249	277000	270939
				1223	1364	−0.0128	0.101	270254	263486
7C 021929.69+424830.00	0.34	12863/12612	Furniss/Stocke	1132	1798	−0.0862	0.451	109477	−23886
QSO B2356−309	0.16539	12864	Fang	1132	1469	−0.0862	0.186	71514	−5206
PG 1216+069	0.331	12903	Ho	1132	1798	−0.0862	0.451	107721	−25893
[LB2005] NGC 891 X4	1.181	12904	Bregman	1132	1274	−0.0862	0.0284	210260	190731
				1291	1433	0.0421	0.157	188346	168159
2EUVE J0005−50.0	0.03328	12936	Jenkins	1150	1292	−0.0717	0.0429	31996	−2786
				1309	1568	0.0566	0.266	−6704	−60007
				1589	1764	0.283	0.424	−63826	−92974
ESO 141−55	0.03711	12936	Jenkins	1150	1292	−0.0717	0.0429	33092	−1677
				1309	1568	0.0566	0.266	−5595	−58942
				1589	1764	0.283	0.424	−62766	−91970
2MASX J21362313−6224008	0.05856	12936	Jenkins	1150	1292	−0.0717	0.0429	39140	4460
				1309	1568	0.0566	0.266	541	−53019
				1589	1764	0.283	0.424	−56873	−86376
2MASX J21384992−3828403	0.18299	12936	Jenkins	1150	1292	−0.0717	0.0429	71291	37579
				1309	1568	0.0566	0.266	33716	−20234
				1589	1764	0.283	0.424	−24200	−54947
2MASS J23215113−7026441	0.3	12936	Jenkins	1150	1292	−0.0717	0.0429	97308	65006
				1309	1568	0.0566	0.266	61261	8010
				1589	1764	0.283	0.424	4023	−27224
2MASS J14103839+2304474	0.79581	12958	Tejos	1159	1301	−0.0644	0.0502	171797	146995
				1318	1590	0.0639	0.283	144020	97072
				1611	1786	0.3	0.442	93536	64807
[VV2006] J024500.8−300723	0.34	12988	Bowen	1132	1469	−0.0862	0.186	109477	36467
QSO B0244−3020	0.522	12988	Bowen	1132	1469	−0.0862	0.186	140933	73313
[VV2000] J024337.7−303048	0.66929	12988	Bowen	1132	1469	−0.0862	0.186	161551	98704
QSO B0246−308	1.093	12988	Bowen	1132	1469	−0.0862	0.186	203804	154099
9C J1001+2911	0.08597	13008	Stocke	1132	1798	−0.0862	0.451	51250	−84593
4C 21.35	0.43351	13008	Stocke	1132	1798	−0.0862	0.451	126556	−3714
3FGL J2345.2−1554	0.621	13008	Stocke	1132	1798	−0.0862	0.451	155208	33001
ESO 350−38	0.020598	13017	Heckman	1150	1292	−0.0717	0.0429	28332	−6487
				1309	1602	0.0566	0.293	−10403	−69666
				1623	1798	0.31	0.451	−73348	−101408
LBQS 1340−0038	0.326537	13033	Tumlinson	1068	1798	−0.138	0.451	121749	−26892
2MASS J13304515+2813216	0.41731	13033	Tumlinson	1132	1798	−0.0862	0.451	123743	−7120

Table 1: (continued)

QSO	z_{em}	COS Prop ID	PI Name	λ_{down} ()	λ_{up} ()	$z_{down,\ N\ V}$	$z_{up,\ N\ V}$	$v_{down,\ N\ V}$ (km s^{-1})	$v_{up,\ N\ V}$ (km s^{-1})
Ton 730	0.08655	13314	Borthakur	1068	1208	−0.138	−0.0249	68154	32312
				1223	1364	−0.0128	0.101	28651	−3973
2MASX J14261331+1955244	0.21328	13314	Borthakur	1068	1208	−0.138	−0.0249	98630	64488
				1223	1364	−0.0128	0.101	60950	29009
2MASX J13485478+4303095	0.27423	13314	Borthakur	1068	1208	−0.138	−0.0249	111516	78345
				1223	1364	−0.0128	0.101	74887	43485
2MASX J13391241+5355278	0.29328	13314	Borthakur	1150	1292	−0.0717	0.0429	95915	63523
				1309	1451	0.0566	0.171	59770	29609
[VV98] J142455.6+421405	0.31585	13314	Borthakur	1068	1208	−0.138	−0.0249	119717	87245
				1223	1364	−0.0128	0.101	83846	52871
[VV2006] J102512.8+480852	0.33158	13314	Borthakur	1132	1274	−0.0862	0.0284	107835	75777
				1291	1433	0.0421	0.157	72045	41921
2MASSI J1017309+470225	0.3348	13314	Borthakur	1150	1292	−0.0717	0.0429	104331	72508
				1309	1451	0.0566	0.171	68807	38958
[VV2006] J140854.2+565743	0.33628	13314	Borthakur	1132	1274	−0.0862	0.0284	108754	76765
				1291	1433	0.0421	0.157	73039	42956
[VV2006] J110236.7+052117	0.49874	13314	Borthakur	1132	1274	−0.0862	0.0284	137310	107857
				1291	1433	0.0421	0.157	104381	75960
[VV2006] J102056.3+100333	0.60744	13314	Borthakur	1132	1274	−0.0862	0.0284	153357	125653
				1291	1433	0.0421	0.157	122359	95230
2MASS J14285904+3225067	0.62704	13314	Borthakur	1132	1274	−0.0862	0.0284	156023	128633
				1291	1433	0.0421	0.157	125372	98484
[VV98] J134447.8+554656	0.93693	13314	Borthakur	1150	1292	−0.0717	0.0429	187796	165030
				1309	1451	0.0566	0.171	162279	139248
[VV2006] J112632.9+120437	0.97582	13314	Borthakur	1150	1292	−0.0717	0.0429	191372	169139
				1309	1451	0.0566	0.171	166447	143879
2MASS J08415917+1406422	1.25143	13314	Borthakur	1132	1274	−0.0862	0.0284	214994	196288
				1291	1433	0.0421	0.157	193998	174573
QSO B1258+2835	1.3597	13314	Borthakur	1132	1451	−0.0862	0.171	221606	181269
2MASS J10474176+1513324	0.38534	13342	Wang	1132	1775	−0.0862	0.433	118015	−10098
ESO 499−41	0.01291	13347	Bregman	1132	1798	−0.0862	0.451	30770	−103410
Mrk 1253	0.049	13347	Bregman	1132	1798	−0.0862	0.451	41114	−94054
2MASX J10053271−2417161	0.15353	13347	Bregman	1132	1798	−0.0862	0.451	68615	−67673
2XMM J100420.0+051300	0.16012	13347	Bregman	1068	1798	−0.138	0.451	86481	−66050
2MASS J10155924−2748289	0.2388	13347	Bregman	1132	1798	−0.0862	0.451	88516	−47086
2E 1259.0+2807	0.2425	13382	Putman	1132	1451	−0.0862	0.171	89332	17677
2MASS J12584666+2427392	0.37107	13382	Putman	1132	1451	−0.0862	0.171	115382	46830
[VV2000] J130346.0+263314	0.43556	13382	Putman	1132	1451	−0.0862	0.171	126908	60168
QSO J1304+2454	0.60241	13382	Putman	1132	1451	−0.0862	0.171	152662	90999
Ton 133	0.65253	13382	Putman	1132	1451	−0.0862	0.171	159393	99302
US 218	0.80407	13382	Putman	1132	1451	−0.0862	0.171	177376	122001
LB 11394	0.82265	13382	Putman	1132	1451	−0.0862	0.171	179360	124553
Ton 694	1.30979	13382	Putman	1132	1451	−0.0862	0.171	218653	177150
2MASX J12323585+0603096	0.08347	13383	Putman	1132	1786	−0.0862	0.442	50579	−83380

Table 1: (continued)

QSO	z_{em}	COS Prop ID	PI Name	λ_{down} ()	λ_{up} ()	$z_{down,\ N\ V}$	$z_{up,\ N\ V}$	$v_{down,\ N\ V}$ (km s^{-1})	$v_{up,\ N\ V}$ (km s^{-1})
2E 2135.0−1446	0.19993	13398	Churchill	1068	1579	−0.138	0.275	95661	−18076
				1600	1775	0.292	0.433	−22019	−52626
2MASX J15474353+2052167	0.26461	13398	Churchill	1068	1602	−0.138	0.293	109553	−6693
				1623	1798	0.31	0.451	−10594	−41037
QSO B2128−123	0.501	13398	Churchill	1132	1274	−0.0862	0.0284	137667	108250
				1291	1602	0.0421	0.293	104778	44353
				1623	1798	0.31	0.451	40527	10074
2MASS J08533423+4349023	0.51419	13398	Churchill	1068	1579	−0.138	0.275	153010	51134
				1600	1775	0.292	0.433	47280	16544
2MASS J03512857−1429082	0.614	13398	Churchill	1168	1310	−0.0572	0.0575	147245	119715
				1327	1579	0.0712	0.275	116450	69490
				1600	1775	0.292	0.433	65731	35530
ICRF J135704.4+191907	0.71956	13398	Churchill	1382	1556	0.116	0.256	122187	91188
				1577	1752	0.273	0.414	87526	57865
3C 454.3	0.859001	13398	Churchill	1141	1283	−0.079	0.0357	181621	157777
				1300	1602	0.0494	0.293	154904	104270
				1623	1798	0.31	0.451	100822	72727
QSO J0125−0005	1.07454	13398	Churchill	1405	1798	0.134	0.451	161826	102759
QSO B1641+394	2.35384	13398	Churchill	1159	1301	−0.0644	0.0502	256504	246252
				1318	1602	0.0639	0.293	244973	222189
				1611	1798	0.3	0.451	221429	205217
[VV2000] J100610.7+370513	3.20092	13415	Syphers	1068	1442	−0.138	0.164	275561	257041
2MASS J15443053+2827567	0.23236	13423	Cooke	1168	1310	−0.0572	0.0575	78418	45532
				1327	1469	0.0712	0.186	41749	11539
2MASSI J1456086+275008	0.24821	13423	Cooke	1159	1301	−0.0644	0.0502	84116	51276
				1318	1460	0.0639	0.179	47490	17199
2E 4626	0.32571	13423	Cooke	1168	1310	−0.0572	0.0575	98393	66646
				1327	1469	0.0712	0.186	62961	33297
2MASSI J1419167+320302	0.38522	13423	Cooke	1168	1310	−0.0572	0.0575	109965	79030
				1327	1469	0.0712	0.186	75422	46227
2MASS J09042330+4007046	0.41006	13423	Cooke	1394	1568	0.125	0.266	66513	32250
				1589	1764	0.283	0.424	28302	−2935
2MASS J14545002+1114344	0.4675	13423	Cooke	1405	1579	0.134	0.275	75586	41972
				1600	1775	0.292	0.433	38082	7170
[VV2000] J101030.6+255948	0.51153	13423	Cooke	1394	1568	0.125	0.266	85989	52656
				1589	1764	0.283	0.424	48782	17876
PB 3734	0.52209	13423	Cooke	1382	1556	0.116	0.256	90263	56900
				1577	1752	0.273	0.414	53016	21991
2MASX J12193086+0643348	0.08044	13444	Wakker	1132	1469	−0.0862	0.186	49763	−27816
2MASX J23345253−3538417	0.098	13444	Wakker	1132	1469	−0.0862	0.186	54450	−23018
LEDA 3096742	0.11	13444	Wakker	1132	1469	−0.0862	0.186	57595	−19776
6dFGS gJ230152.0−550831	0.14	13444	Wakker	1132	1469	−0.0862	0.186	65254	−11804
2MASS J13534104+3619480	0.14662	13444	Wakker	1132	1469	−0.0862	0.186	66905	−10070
2MASX J13532610+3620492	0.28491	13444	Wakker	1132	1469	−0.0862	0.186	98406	24012

Table 1: (continued)

QSO	$z_{\rm em}$	COS Prop ID	PI Name	$\lambda_{\rm down}$ ()	$\lambda_{\rm up}$ ()	$z_{\rm down,\ N\ V}$	$z_{\rm up,\ N\ V}$	$v_{\rm down,\ N\ V}$ (km s^{-1})	$v_{\rm up,\ N\ V}$ (km s^{-1})
[VV2000] J230222.5−550827	0.851	13444	Wakker	1132	1469	−0.0862	0.186	182304	125323
ESO 462−9	0.019466	13448	Fox	1132	1274	−0.0862	0.0284	32683	−2615
				1291	1579	0.0421	0.275	−6588	−65868
				1600	1775	0.292	0.433	−69626	−98272
Mrk 1392	0.03588	13448	Fox	1132	1274	−0.0862	0.0284	37406	2173
				1291	1579	0.0421	0.275	−1800	−61295
				1600	1775	0.292	0.433	−65080	−93976
Mrk 841	0.03642	13448	Fox	1132	1274	−0.0862	0.0284	37559	2330
				1291	1579	0.0421	0.275	−1644	−61145
				1600	1775	0.292	0.433	−64931	−93835
6dFGS gJ161519.1−093613	0.06496	13448	Fox	1132	1274	−0.0862	0.0284	45546	10469
				1291	1579	0.0421	0.275	6499	−53299
				1600	1775	0.292	0.433	−57125	−86428
6dFGS gJ200553.0−413442	0.07963	13448	Fox	1132	1274	−0.0862	0.0284	49545	14564
				1291	1579	0.0421	0.275	10597	−49317
				1600	1775	0.292	0.433	−53162	−82653
2XMM J135435.6+180518	0.15087	13448	Fox	1132	1274	−0.0862	0.0284	67959	33590
				1291	1579	0.0421	0.275	29660	−30507
				1600	1775	0.292	0.433	−34421	−64660
2FHL J2324.7−4041	0.17359	13448	Fox	1132	1274	−0.0862	0.0284	73493	39364
				1291	1579	0.0421	0.275	35452	−24696
				1600	1775	0.292	0.433	−28625	−59049
QSO B1725−142	0.184	13448	Fox	1132	1274	−0.0862	0.0284	75976	41963
				1291	1579	0.0421	0.275	38060	−22065
				1600	1775	0.292	0.433	−26000	−56499
[VV96] J232210.8−344757	0.42	13448	Fox	1132	1274	−0.0862	0.0284	124214	93507
				1291	1579	0.0421	0.275	89905	32260
				1600	1775	0.292	0.433	28339	−2693
[VV2006] J104923.2+021806	0.74908	13473	Heckman	1132	1274	−0.0862	0.0284	171234	145763
				1291	1590	0.0421	0.283	142709	89937
				1611	1786	0.3	0.442	86343	57231
[VV2006] J142614.8+004159	0.89631	13473	Heckman	1068	1208	−0.138	−0.0249	197094	174404
				1223	1364	−0.0128	0.101	171939	148621
				1382	1556	0.116	0.256	145637	116958
				1577	1752	0.273	0.414	113533	85495
QSO B1035+043	1.08689	13473	Heckman	1150	1292	−0.0717	0.0429	200750	179971
				1309	1556	0.0566	0.256	177444	140352
				1577	1752	0.273	0.414	137194	111092
QSO J1419+0606	1.63768	13473	Heckman	1132	1274	−0.0862	0.0284	235545	220675
				1291	1579	0.0421	0.275	218837	186288
				1600	1775	0.292	0.433	183837	163180
HS 1700+6416	2.73745	13491	Tripp	1068	1469	−0.138	0.186	269502	244956
Mrk 1502	0.0589	15569	Martin	1150	1469	−0.0717	0.186	39235	−33790

Table 2: Sample Quasars and Their Properties

QSO	$z_{\rm em}$	$\log(L_\nu(3000\ ))$ (erg s^{-1} Hz^{-1})	$\log(L_\nu(\rm radio))$ erg s^{-1} Hz^{-1}	ν (GHz)	$\log(L_\nu(5\ \rm GHz))$ erg s^{-1} Hz^{-1}	$\log(\mathcal{R})$	L/Q	$v_{\rm down}$(N v) (km s^{-1})	$v_{\rm up}$(N v) (km s^{-1})
NGC−4395	0.001064	3.61E+27	2.91E+25	1.4	1.19E+25	−2.48	quiet	27277	−106504
NGC−4051	0.002336	1.46E+28	2.32E+27	1.4	9.53E+26	−1.19	quiet	27129	−100226
NGC−4151	0.003319	1.59E+28	5.34E+27	1.4	2.19E+27	−0.86	quiet	27946	−105915
NGC−3227	0.003859	3.11E+28	2.71E+28	1.4	1.12E+28	−0.45	quiet	23411	−104012
IRAS23133−4251	0.005365	5.25E+28	1.75E+29	1.49	7.52E+28	0.16	quiet	26197	−47248
NGC−3259	0.005624	8.85E+27	5.29E+27	1.4	2.18E+27	−0.61	quiet	−40671 −77498	−73843 −105312
NGC−3516	0.008836	4.52E+28	5.39E+28	1.4	2.22E+28	−0.31	quiet	29574	−104473
NGC−3783	0.00973	4.82E+28	9.11E+28	1.4	3.76E+28	−0.11	quiet	29837	−104240
ESO−499−41	0.01291	1.98081E+28	2.50E+28	1.4	1.27E+27	−0.41	quiet	30770	−103410
ESO267−013	0.01488	2.82E+28	...	...	...	...	...	31347	−46290
NGC−7469	0.016317	9.80E+28	8.59E+29	1.4	3.56E+29	0.56	quiet	31766	−102522
MRK−1044	0.016451	1.25E+28	7.01E+27	1.4	2.91E+27	−0.63	quiet	31805	−102487
NGC−5548	0.017175	8.25E+28	1.60E+29	1.4	6.62E+28	−0.1	quiet	32016	−102299
NGC1275	0.017559	1.58E+29	1.56E+32	1.4	6.48E+31	2.61	loud	−32392 −70157	−66402 −98773
ESO−462−9	0.019466	4.09099E+28	2.72E+28	1.4	1.70E+27	−0.69	quiet	32683 −6588 −69626	−2615 −65868 −98272
HARO11	0.020598	7.51E+28	2.52E+29	1.4	1.05E+29	0.15	quiet	28332 −10403 −73348	−6487 −69666 −101408
AKN−564	0.024684	5.43E+28	3.88E+29	1.4	1.62E+29	0.47	quiet	34194	−100346
MRK335	0.025785	1.24E+29	1.08E+29	1.4	4.51E+28	−0.44	quiet	33468	−97972
KAZ147	0.0266	1.66E+28	<3.94E+28	1.4	<1.65E+28	<0	quiet	34747	−42924
MRK595	0.026982	5.46E+28	<7.00E+27	1.4	<2.93E+27	<−1.27	quiet	34857	−42815
SDSS−J004042.09−110957.7	0.027405	4.49E+27	<6.67E+27	1.4	<2.79E+27	<−0.21	quiet	−34348 −71471	−67778 −99639
ESO031−−G−008	0.027619	4.94E+28	...	...	...	...	...	35040 −4201 −67363	−227 −63591 −96135
SDSSJ172243.80+620958.0	0.028341	6.95E+28	<7.68E+27	1.4	<3.21E+27	<−1.34	quiet	35248	−42426
SDSSJ172823.40+573243.0	0.02835	5.28E+28	2.15E+29	1.4	8.98E+28	0.23	quiet	35251	−42424
UGC10855	0.02856	...	<8.12E+27	1.4	<3.40E+27	...	...	35311	−42364
MRK290	0.029577	5.24E+28	1.04E+29	1.4	4.34E+28	−0.08	quiet	34821	−96982
MRK421	0.030021	2.55E+29	1.15E+31	1.4	4.83E+30	1.28	loud	35731	−96867
KAZ49	0.030097	4.07E+28	<8.54E+27	1.4	<3.58E+27	<−1.06	quiet	35752	−41925
MRK−279	0.030451	8.16E+28	4.80E+29	1.4	2.01E+29	0.39	quiet	35854	−98849
MRK817	0.031455	9.29E+28	2.03E+29	1.4	8.52E+28	−0.04	quiet	35359	−98588
2EUVE−J0005−50.0	0.03328	6.19829E+29	<2.00E+29	0.843	<1.64E+28	<−0.89	quiet	31996 −6704 −63826	−2786 −60007 −92974
MRK0509	0.034397	4.44E+29	4.92E+29	1.4	2.07E+29	−0.33	quiet	32317	−90826
MCG−02−16−004	0.035558	2.99E+28	2.09E+29	1.4	8.80E+28	0.47	quiet	37314	−40370

Table 2: (continued)

QSO	$z_{\rm em}$	$\log(L_\nu(3000\ ))$ (erg s^{-1} Hz^{-1})	$\log(L_\nu(\rm radio))$ erg s^{-1} Hz^{-1}	ν (GHz)	$\log(L_\nu(5\ \rm GHz))$ erg s^{-1} Hz^{-1}	$\log(\mathcal{R})$	L/Q	$v_{\rm down}$(N v) (km s^{-1})	$v_{\rm up}$(N v) (km s^{-1})
MRK504	0.035888	1.21E+28	<1.30E+28	1.4	<5.45E+27	<−0.35	quiet	37408	−40276
ESO−141−55	0.03711	2.90526E+29	<2.49E+29	0.843	<2.15E+28	<−0.47	quiet	33092 −5595 −62766	−1677 −58942 −91970
MRK486	0.038934	7.53E+28	4.18E+28	1.4	1.76E+28	−0.63	quiet	38274	−39411
HS1831+5338	0.039	3.96E+28	<8.52E+28	1.4	<3.59E+28	<−0.04	quiet	38293	−39392
HE0429−5343	0.040008	1.19E+28	...	...	...	...	...	29314 −8851	−4988 −39107
QSOB1254+571	0.04217	1.83E+29	9.68E+30	1.4	4.09E+30	1.35	loud	34533	−38495
2MASXJ01414319+1340328	0.045	9.25126E+28	1.43E+29	1.4	1.36E+28	−0.33	quiet	39990	−37695
UM428	0.046399	1.09E+29	4.06E+29	1.4	1.72E+29	0.2	quiet	40384	−37300
ESO113−45	0.048175	4.15683E+29	<4.23E+29	0.843	<4.15E+28	<−0.40	quiet	40883 1737 −59717	5710 −55877 −89079
Mrk1253	0.049	1.13411E+30	<5.25E+28	1.4	<5.20E+27	<−1.85	quiet	41114	−94054
NVSSJ15251−1714	0.049651	2.51E+29	2.42E+30	1.4	1.03E+30	0.61	quiet	41297	−36384
ESO265−G23	0.056576	1.53E+29	...	...	...	...	...	34000 −4115	−250 −34440
PG1011−040	0.058314	1.32E+29	<3.39E+28	1.4	<1.45E+28	<−0.96	quiet	43711	−89835
2MASXJ21362313−6224008	0.05856	1.84004E+29	5.03E+29	0.843	5.44E+28	0.03	quiet	39140 541 −56873	4460 −53019 −86376
NPM1G+68.0125	0.058637	1.37E+29	2.33E+29	1.4	9.96E+28	−0.14	quiet	43801	−33863
QSOB0050+124	0.0589	3.81E+29	4.30E+29	1.4	1.84E+29	−0.32	quiet	39235	−33790
QSO−B1126−041	0.06196	2.34E+29	1.07E+29	1.4	4.58E+28	−0.71	quiet	40085	−32935
2MASXJ01002713−5113544	0.06282	1.6896E+29	<7.25E+29	0.843	<8.13E+28	<0.22	quiet	44957 5896 −55712	9867 −51852 −85271
MRK1513	0.062977	3.50E+29	4.69E+29	1.4	2.01E+29	−0.24	quiet	45000	−90462
QSOB1229+204	0.06301	1.91E+29	<4.00E+28	1.4	<1.71E+28	<−1.05	quiet	40376	−32643
MR2251−178	0.06398	4.51E+29	1.50E+30	1.4	6.44E+29	0.15	quiet	45277	−90205
CAL−F	0.064	3.20E+29	2.08E+30	0.843	6.25E+29	0.29	quiet	45282 6228 −53192	8091 −51529 −84965
QSO−B0844+349	0.064	1.34E+30	<3.93E+28	1.4	<1.68E+28	<−1.9	quiet	40650	−32367
IRAS23365+3604	0.06448	7.68E+28	2.56E+30	1.4	1.10E+30	1.16	loud	36203 −1881	1984 −32233
6dFGSgJ161519.1−093613	0.06496	2.6705E+29	<2.42E+29	1.4	<2.76E+28	<−0.56	quiet	45546 6499 −57125	10469 −53299 −86428
SDSSJ145108.76+270926.9	0.065	2.56E+29	3.58E+29	1.4	1.54E+29	−0.22	quiet	45557	−89943
QSO−B2214+139	0.065762	3.56E+29	<4.42E+28	1.4	<1.89E+28	<−1.27	quiet	45767 −54911	−51047 −84508
SBS1624+575	0.067	4.20E+28	<4.56E+28	1.4	<1.96E+28	<−0.33	quiet	46107	−31532

Table 2: (continued)

QSO	$z_{\rm em}$	$\log(L_\nu(3000\ ))$ (erg s^{-1} Hz^{-1})	$\log(L_\nu(\rm radio))$ erg s^{-1} Hz^{-1}	ν (GHz)	$\log(L_\nu(5\ \rm GHz))$ erg s^{-1} Hz^{-1}	$\log(\mathcal{R})$	L/Q	$v_{\rm down}$(N v) (km s^{-1})	$v_{\rm up}$(N v) (km s^{-1})
RBS563	0.069	1.54E+29	...	...	...	...	...	46655 7633 −51830	9495 −50164 −83671
4C10.08	0.07	7.23E+28	<2.79E+29	1.4	<1.20E+29	<0.22	quiet	46928	−30700
PKS2005−489	0.071	2.35E+29	1.22E+32	2.7	8.29E+31	2.55	loud	46427	−86418
MCG+10−22−028	0.073424	1.94E+29	<5.60E+28	1.4	<2.41E+28	<−0.91	quiet	47862	−29752
SDSSJ170328.90+614109.0	0.077319	1.13E+29	<6.38E+28	1.4	<2.76E+28	<−0.61	quiet	48919	−28676
SBS1518+593	0.0781	2.01E+29	<6.35E+28	1.4	<2.74E+28	<−0.86	quiet	49131	−28461
QSO−B1440+3539	0.079055	4.06E+29	4.77E+29	1.4	2.06E+29	−0.29	quiet	44776	−28198
TON1187	0.079097	2.98E+29	<5.83E+28	1.4	<2.52E+28	<−1.07	quiet	40225 2208	6072 −28186
6dFGSgJ200553.0−413442	0.07963	3.35338E+28	<2.64E+30	0.843	<3.33E+29	<1.48	?	−14755 −53162	−49317 −82653
SDSSJ031027.82−004950.7	0.080139	1.47E+29	<6.34E+28	1.4	<2.74E+28	<−0.73	quiet	49682	−86077
2XMMJ121930.9+064334	0.08044	1.48977E+29	4.90E+29	1.4	6.21E+28	−0.01	quiet	49763	−27816
2MASXJ12323585+0603096	0.08347	9.14376E+28	<1.52E+29	1.4	<1.96E+28	<−0.30	quiet	50579	−83380
9C−J1001+2911	0.08597	1.953E+28	2.50E+31	1.4	3.28E+30	2.58	loud	51250	−84593
2MASXJ13435674+2538474	0.08655	1.9157E+29	<1.72E+29	1.4	<2.27E+28	<−0.57	quiet	68154 28651	32312 −3973
QSO−B1351+6400	0.0882	5.64E+29	4.80E+30	1.4	2.09E+30	0.57	quiet	47247	−25688
QSOB0007+107	0.089338	3.46E+29	2.82E+31	1.4	1.23E+31	1.55	loud	47552	−25377
QSO−B1411+4414	0.0896	5.07E+29	4.48E+29	1.4	1.95E+29	−0.42	quiet	47623	−25305
2MASXJ23345253−3538417	0.098	8.87458E+28	<5.60E+29	1.4	<7.84E+28	<0.27	quiet	54450	−23018
SBS1527+564	0.099	1.73E+29	1.02E+30	1.4	4.45E+29	0.41	quiet	54714	−22747
PG0804+761	0.1	1.62E+30	7.61E+29	1.4	3.34E+29	−0.69	quiet	54978	−81039
IRAS−F22456−5125	0.1	3.22E+29	...	...	...	...	...	54978	−81039
UKS0242−724	0.1018	2.86E+29	...	...	...	...	...	55451 16678 −47240	20636 −43369 −76991
IRAS−F04250−5718	0.104	1.57E+30	4.67E+30	0.843	1.44E+30	−0.04	quiet	56029	−80029
HE2332−3556	0.11	1.15363E+29	<7.10E+29	1.4	<1.05E+29	<0.26	quiet	57595	−19776
QSOB1617+1731	0.112438	5.29E+29	<1.64E+29	1.4	<7.26E+28	<−0.86	quiet	58228	−15437
RXSJ15032+6809	0.114	9.12E+28	<7.53E+29	1.4	<3.33E+29	<0.56	quiet	58633	−18702
TONS210	0.116	1.14E+30	<7.81E+29	1.4	<3.46E+29	<−0.52	quiet	59150	−77010
QSOB2155−304	0.116	5.0781E+30	1.55E+32	1.4	2.36E+31	0.95	quiet	59150 −43489	−39604 −73394
RXJ1230.8+0115	0.117	1.50E+30	<6.10E+29	1.4	<2.70E+29	<−0.74	quiet	59408	−76760
HS−0033+4300	0.12	1.22E+29	<8.37E+29	1.4	<3.72E+29	<0.48	quiet	59165 21800 −38363	25519 −34595 −65915
MRK106	0.123366	4.34E+29	<1.34E+29	1.4	<5.96E+28	<−0.86	quiet	61043	−75165
QSOB1435−0645	0.126	6.24E+29	<2.08E+29	1.4	<9.25E+28	<−0.83	quiet	61716	−11812
SDSSJ152139.66+033729.2	0.1265	1.66E+29	<1.67E+29	1.4	<7.43E+28	<−0.35	quiet	61843 −36468	−34776 −68986

Table 2: (continued)

QSO	$z_{\rm em}$	$\log(L_\nu(3000\ ))$ (erg s^{-1} Hz^{-1})	$\log(L_\nu(\rm radio))$ erg s^{-1} Hz^{-1}	ν (GHz)	$\log(L_\nu(5\ \rm GHz))$ erg s^{-1} Hz^{-1}	$\log(\mathcal{R})$	L/Q	$v_{\rm down}$(N v) (km s^{-1})	$v_{\rm up}$(N v) (km s^{-1})
IRAS−L06229−6434	0.128889	5.48E+30	2.06E+32	4.85	2.19E+32	1.6	loud	62451 24156 −35842	25776 −34149 −68384
MRK876	0.129	8.72E+29	1.51E+30	1.4	6.76E+29	−0.11	quiet	62479 24648	25805 −71076
VIIZW244	0.131	3.36E+29	<1.00E+30	1.4	<4.48E+29	<0.12	quiet	62480	−71052
PG1626+554	0.133	3.92E+29	<1.83E+29	1.4	<8.21E+28	<−0.68	quiet	63493	−72761
QSO0045+3926	0.134	2.94E+29	<1.05E+30	1.4	<4.70E+29	<0.2	quiet	63745	−72512
PKS0558−504	0.1372	1.26E+30	8.37E+31	2.7	5.95E+31	1.67	loud	64046 26340 −33860	30048 −30080 −61387
SDSSJ094733.21+100508.7	0.13954	4.27E+29	8.21E+29	1.4	3.69E+29	−0.06	quiet	65139	−71135
6dFGSgJ230152.0−550831	0.14	8.99603E+29	<3.73E+30	0.843	<6.24E+29	<0.19	quiet	65254	−11804
QSOB0026+129	0.142	9.05E+29	3.36E+30	1.4	1.51E+30	0.22	quiet	65754	−7587
2MASSJ13534104+3619480	0.14662	1.90043E+29	<7.63E+28	1.4	<1.31E+28	<−0.93	quiet	66905	−10070
SDSSJ135712.61+170444.1	0.1505	1.51E+29	<2.14E+29	1.4	<9.69E+28	<−0.19	quiet	67867	−68421
2XMMJ135435.6+180518	0.15087	4.77376E+29	<5.49E+29	1.4	<9.53E+28	<−0.48	quiet	67959 29660 −34421	33590 −30507 −64660
SDSSJ112114.22+032546.7	0.151994	2.04E+29	1.20E+30	1.4	5.42E+29	0.42	quiet	68236	−68052
2MASXJ10053271−2417161	0.15353	3.0758E+30	<1.41E+30	1.4	<2.47E+29	<−0.88	quiet	68615	−67673
PG1115+407	0.154338	7.65E+29	1.30E+30	1.4	5.90E+29	−0.11	quiet	68814	−67474
QSOB1307+085	0.155	1.02E+30	<2.55E+29	1.4	<1.16E+29	<−0.94	quiet	64481	−7889
RXSJ09565−0452	0.1571	1.45E+30	1.04E+30	1.4	4.71E+29	−0.49	quiet	69492	−7345
PG1226+023	0.158	1.18971E+31	3.19E+34	1.4	5.67E+33	2.89	loud	69712	−5270
7C−1424+2401	0.16	2.14729E+30	2.54E+32	1.4	4.54E+31	1.53	loud	70202	−66079
2XMMJ100420.0+051300	0.16012	5.19823E+29	<6.14E+29	1.4	<1.10E+29	<−0.47	quiet	86481	−66050
SDSSJ095915.65+050355.1	0.162631	2.58E+29	<2.81E+29	1.4	<1.28E+29	<−0.3	quiet	66361	−61747
QSOB0157+001	0.16311	9.43E+29	1.44E+31	1.4	6.57E+30	0.84	quiet	66479	−5793
2MASSJ15442726+2743242	0.16392	2.46369E+29	<6.25E+29	1.4	<1.13E+29	<−0.13	quiet	66677	−5584
SDSSJ135625.55+251523.7	0.164009	6.02E+29	<2.69E+29	1.4	<1.23E+29	<−0.69	quiet	71178 −26758	−25055 −59619
2MASSJ00583738−3606048	0.16414	1.99962E+30	<1.62E+30	1.4	<2.93E+29	<−0.63	quiet	71210 33060 −28978	36979 −25022 −59587
SDSSJ015530.02−085704.0	0.164427	3.48E+29	<1.60E+30	1.4	<7.29E+29	<0.32	quiet	71280	−64992
PG1202+281	0.1653	2.67E+29	<3.01E+29	1.4	<1.37E+29	<−0.29	quiet	67015	−61088
QSOB2356−309	0.16539	4.92064E+29	4.08E+31	1.4	7.42E+30	1.38	loud	71514	−5206
PG1048+342	0.167008	3.95E+29	<2.89E+29	1.4	<1.32E+29	<−0.48	quiet	71906	−64359
SDSSJ121114.56+365739.5	0.171084	4.56E+29	<3.08E+29	1.4	<1.41E+29	<−0.51	quiet	72890	−63361
SDSSJ134231.22+382903.4	0.171894	2.42E+29	<3.05E+29	1.4	<1.40E+29	<−0.24	quiet	73085	−63163
[VV2000]J103216.1+505120	0.17314	1.7327E+29	<1.00E+29	1.4	<1.87E+28	<−0.78	quiet	73385	−62859
2MASSJ23244467−4040493	0.17359	1.58021E+30	3.66E+31	0.843	6.83E+30	0.94	quiet	73493 35452	39364 −24696

Table 2: (continued)

QSO	$z_{\rm em}$	$\log(L_\nu(3000\ ))$ (erg s^{-1} Hz^{-1})	$\log(L_\nu(\rm radio))$ erg s^{-1} Hz^{-1}	ν (GHz)	$\log(L_\nu(5\ \rm GHz))$ erg s^{-1} Hz^{-1}	$\log(\mathcal{R})$	L/Q	$v_{\rm down}$(N v) (km s^{-1})	$v_{\rm up}$(N v) (km s^{-1})
								−28625	−59049
4C−−01.61	0.17374	1.18E+30	3.19E+32	1.4	1.46E+32	2.09	loud	69067	−3066
SDSSJ021218.32−073719.8	0.17392	1.97E+29	<3.40E+29	1.4	<1.56E+29	<−0.1	quiet	73572	−62668
RXSJ16083+6018	0.178	7.52E+29	4.25E+31	1.4	1.95E+31	1.41	loud	74549	−1980
SDSSJ113137.16+155645.3	0.18289	2.03095E+29	<7.28E+29	1.4	<1.39E+29	<0.01	quiet	73486	−738
QSOB1309+3531	0.182923	1.20E+30	3.56E+31	1.4	1.64E+31	1.13	loud	75720	2967
2MASXJ21384992−3828403	0.18299	6.94967E+29	<2.02E+30	1.4	<3.87E+29	<−0.08	quiet	71291 33716 −24200	37579 −20234 −54947
QSOB1725−142	0.184	5.68988E+30	1.83E+31	1.4	3.52E+30	−0.03	quiet	75976 38060 −26000	41963 −22065 −56499
PMNJ1103−2329	0.186	9.94E+29	9.92E+31	1.4	4.58E+31	1.66	loud	76449	−59727
2MASX−J01013113+4229356	0.19	...	<2.15E+30	1.4	<9.98E+29	...	...	76898 39778 −20179	42987 −16750 −50917
PHL1811	0.19	5.47E+30	5.25E+29	1.4	2.43E+29	−1.35	quiet	77392	−58757
QSOB0923+201	0.192142	1.61E+30	<3.65E+29	1.4	<1.69E+29	<−0.98	quiet	77895	5293
2MASSJ22452029−4652116	0.198	3.27784E+30	<1.71E+31	0.843	<3.41E+30	<0.28	quiet	79264 41521 −20441	45412 −16468 −51286
2E−2135.0−1446	0.19993	2.09641E+30	<2.43E+30	1.4	<4.86E+29	<−0.48	quiet	95661 −22019	−18076 −52626
QSOB2357−1302	0.2	1.13192E+30	<2.43E+30	1.4	<4.86E+29	<−0.21	quiet	79728 42012 −19944	45900 −15970 −50800
4C63.22	0.204	1.25E+30	1.23E+31	1.4	5.76E+30	0.66	quiet	80655	4565
SDSSJ123604.02+264135.9	0.209152	3.06E+29	<5.80E+29	1.4	<2.72E+29	<−0.05	quiet	75260 38155	39949 −50398
SDSSJ104843.49+130605.9	0.218529	5.85E+28	<4.97E+29	1.4	<2.34E+29	<0.6	quiet	81787 44471 −15366	48322 −11386 −46327
PG1121+422	0.225	1.56E+30	<5.17E+29	1.4	<2.44E+29	<−0.81	quiet	85441	−50355
SDSSJ001224.01−102226.5	0.228191	5.34E+29	4.71E+30	1.4	2.23E+30	0.62	quiet	86157	−49597
SDSSJ122102	0.229453	3.11E+29	<5.61E+29	1.4	<2.66E+29	<−0.07	quiet	84257 47084	50924 16382
SDSSJ161711	0.229454	6.50E+29	<5.88E+29	1.4	<2.79E+29	<−0.37	quiet	86439	−49297
SDSSJ094621	0.230217	2.61E+29	<5.30E+29	1.4	<2.52E+29	<−0.02	quiet	86610	−49116
PG0953+414	0.2341	4.69E+30	<5.05E+29	1.4	<2.40E+29	<−1.29	quiet	87475	−48196
SDSSJ075620	0.235748	6.28E+29	<5.73E+29	1.4	<2.73E+29	<−0.36	quiet	...	...
2MASSJ10155924−2748289	0.2388	7.55564E+29	<3.51E+30	1.4	<7.68E+29	<0.12	quiet	88516	−47086
SDSSJ092909	0.239981	1.36E+30	<6.20E+29	1.4	<2.96E+29	<−0.66	quiet	88777 −14259	−12583 −46807
4C−13.41	0.240613	3.14E+30	1.94E+31	1.4	9.24E+30	0.47	quiet	88916	17223

Table 2: (continued)

QSO	$z_{\rm em}$	$\log(L_\nu(3000\ ))$ (erg s^{-1} Hz^{-1})	$\log(L_\nu(\rm radio))$ erg s^{-1} Hz^{-1}	ν (GHz)	$\log(L_\nu(5\ \rm GHz))$ erg s^{-1} Hz^{-1}	$\log(\mathcal{R})$	L/Q	$v_{\rm down}$(N v) (km s^{-1})	$v_{\rm up}$(N v) (km s^{-1})
SDSSJ133053.27+311930.5	0.24232	5.06E+29	<9.19E+29	1.4	<4.39E+29	<−0.06	quiet	89292 −7309	−5594 −40653
RXJ0439.6−5311	0.243	1.38E+30	...	...	...	...	...	88477	−43969
FBQSJ1010+3003	0.256429	8.27E+29	1.59E+30	1.4	7.63E+29	−0.03	quiet	92367	−42945
SDSSJ115758	0.260247	9.36E+29	<7.63E+29	1.4	<3.68E+29	<−0.41	quiet	93189	−42054
SDSSJ134206.56+050523.8	0.263917	8.03E+29	6.55E+30	1.4	3.16E+30	0.6	quiet	93976	−41199
2MASXJ15474353+2052167	0.26461	3.50357E+30	2.89E+33	1.4	6.64E+32	2.36	loud	109553 −10594	−6693 −41037
SDSSJ122312	0.276924	4.68E+29	<8.23E+29	1.4	<4.01E+29	<−0.07	quiet	94603 58090	61879 27677
PKS1302−102	0.2784	6.05E+30	1.35E+33	1.4	6.58E+32	2.04	loud	97045	−37842
SBS1521+598	0.2862	6.63E+29	<8.81E+29	1.4	<4.31E+29	<−0.19	quiet	98674	24311
SDSSJ122018	0.286705	6.66E+29	<8.79E+29	1.4	<4.30E+29	<−0.19	quiet	96658 60289	64065 29943
TON580	0.289477	2.71E+30	5.97E+32	1.4	2.93E+32	2.03	loud	98883	−35459
SDSSJ104816.25+120734.7	0.29113	1.58E+29	<8.44E+29	1.4	<4.14E+29	<0.42	quiet	97579 61276	65047 30962
SDSSJ171737.95+655939.3	0.292656	7.63E+29	<5.27E+30	1.4	<2.59E+30	<0.53	quiet	100011	25801
SDSSJ092837	0.29589	8.57E+29	<1.02E+30	1.4	<5.00E+29	<−0.23	quiet	99736	−31677
HB891821+643	0.297	1.48E+31	<5.43E+30	1.4	<2.67E+30	<−0.74	quiet	96688 60597 1262	64345 5223 −29757
7C071610.69+712601.00	0.3	1.44587E+31	1.64E+33	1.4	4.02E+32	1.49	loud	101517	−32889
2MASSJ23215113−7026441	0.3	4.96739E+30	<1.81E+31	0.843	<4.43E+30	<0.11	quiet	97308 61261 4023	65006 8010 −27224
PG1112+431	0.301321	8.92E+29	<8.73E+29	1.4	<4.31E+29	<−0.32	quiet	101787	27788
SDSSJ091235	0.305578	6.37E+29	<1.01E+30	1.4	<4.99E+29	<−0.11	quiet	102652	−31621
SDSSJ082633	0.310655	1.38E+30	<1.04E+30	1.4	<5.18E+29	<−0.43	quiet	99491	−26645
SDSSJ120720.99+262429.1	0.322492	1.14E+30	<1.07E+30	1.4	<5.33E+29	<−0.33	quiet	101883	−23969
SDSSJ134251	0.326537	1.54E+30	<1.27E+30	1.4	<6.35E+29	<−0.38	quiet	121749	−26892
PG1001+291	0.327201	3.88E+30	<2.16E+30	1.4	<1.08E+30	<−0.56	quiet	106974	−26743
PG0832+251	0.329684	2.99E+30	4.75E+30	1.4	2.38E+30	−0.1	quiet	107463	−26187
SDSSJ092554.43+453544.4	0.329891	8.26E+29	<1.22E+30	1.4	<6.13E+29	<−0.13	quiet	107504	−26141
SDSSJ132704	0.330398	5.73E+29	<1.11E+30	1.4	<5.58E+29	<−0.01	quiet	103460	−22193
PG1216+069	0.331	6.92481E+30	5.90E+30	1.4	1.52E+30	−0.64	quiet	107721	−25893
2XMMJ150333.9−415224	0.335	3.96E+29	...	...	...	...	...	66037	36370
SBS1458+534	0.338	8.60E+29	<1.28E+30	1.4	<6.43E+29	<−0.13	quiet	109088	36026
7C−021929.69+424830.00	0.34	7.30995E+30	6.75E+33	1.4	1.76E+33	2.40	loud	109477	−23886
7C−021929.69+424830.00	0.34	7.30995E+30	6.75E+33	1.4	1.76E+33	2.40	loud	109477	−23886
SDSSJ121716	0.343511	1.89E+30	<1.33E+30	1.4	<6.72E+29	<−0.45	quiet	108096 72602	76305 42702
RXJ2154.1−4414	0.344	4.28E+30	...	...	...	...	...	110250	−22998
FBS1526+659	0.345	1.75E+30	<7.42E+30	1.4	<3.74E+30	<0.33	quiet	110443	37567

Table 2: (continued)

QSO	$z_{\rm em}$	$\log(L_\nu(3000\ ))$ (erg s^{-1} Hz^{-1})	$\log(L_\nu(\rm radio))$ erg s^{-1} Hz^{-1}	ν (GHz)	$\log(L_\nu(5\ \rm GHz))$ erg s^{-1} Hz^{-1}	$\log(\mathcal{R})$	L/Q	$v_{\rm down}$(N v) (km s^{-1})	$v_{\rm up}$(N v) (km s^{-1})
B0117−2837	0.348858	3.35E+30	<7.59E+30	1.4	<3.84E+30	<0.06	quiet	111184	−21923
PKS1101−325	0.355503	2.65E+30	2.84E+33	1.4	1.44E+33	2.74	loud	112453	39860
SDSSJ150455.56+564920.3	0.358894	1.73E+30	<1.59E+30	1.4	<8.10E+29	<−0.33	quiet	113096	40596
PG1049−005	0.3599	5.25E+30	<1.46E+30	1.4	<7.41E+29	<−0.85	quiet	113286	−15644
1ES1553+113	0.36	9.88E+30	8.16E+32	1.4	4.15E+32	1.62	loud	113305	−19468
2MASXJ10311847+5053358	0.360403	1.74E+30	1.23E+32	1.4	6.27E+31	1.56	loud	113381	−19380
SBS1551+572	0.366	1.62E+30	<1.32E+30	1.4	<6.73E+29	<−0.38	quiet	114434	42129
SDSSJ094952	0.366193	3.14E+30	<1.43E+30	1.4	<7.30E+29	<−0.63	quiet	114470	−18111
RXJ07145+7408	0.371	2.42E+30	3.67E+32	1.4	1.88E+32	1.89	loud	115369	43203
SDSSJ132222.68+464535.2	0.374873	1.32E+30	<1.53E+30	1.4	<7.86E+29	<−0.22	quiet	116088	−16219
SDSSJ122035	0.376654	2.11E+30	7.79E+30	1.4	4.00E+30	0.28	quiet	116418 81370	83094 −15832
SDSSJ024250.85−075914.2	0.377782	1.77E+30	<1.61E+30	1.4	<8.27E+29	<−0.33	quiet	116626	−15587
QSOB1124+271	0.37898	2.08413E+30	6.83E+30	1.4	1.88E+30	−0.06	quiet	116847 23926	27915 −7569
SDSSJ123335	0.38223	1.65E+30	<1.51E+30	1.4	<7.76E+29	<−0.33	quiet	117445	−14623
SDSSJ134246.89+184443.6	0.3832	1.66E+30	<1.64E+30	1.4	<8.43E+29	<−0.29	quiet	117623	−14413
SDSSJ104741.75+151332.2	0.38534	1.16246E+30	<4.07E+30	1.4	<1.13E+30	<−0.03	quiet	118015	−10098
SDSSJ121037.56+315706.0	0.389374	2.99E+30	<1.60E+30	1.4	<8.27E+29	<−0.56	quiet	118751	−13081
PKS0202−76	0.38939	2.30E+30	9.31E+33	1.4	4.81E+33	3.32	loud	118754	−9223
SDSSJ120924	0.395549	2.83E+30	9.26E+30	1.4	4.80E+30	0.23	quiet	117869 83223	86852 53799
SDSSJ104709.83+130454.6	0.400607	7.30E+29	<1.78E+30	1.4	<9.26E+29	<0.1	quiet	118785 84223	87845 54848
SDSSJ110312.93+414154.9	0.403095	3.23E+30	<1.62E+30	1.4	<8.44E+29	<−0.58	quiet	121225	−10139
CSO712	0.405336	1.43E+30	<1.78E+30	1.4	<9.26E+29	<−0.19	quiet	121625	50437
QSOB0901+4019	0.41006	2.25047E+30	<4.24E+30	1.4	<1.22E+30	<−0.30	quiet	66513 28302	32250 −2935
SDSSJ122512	0.411797	1.78E+30	8.85E+31	1.4	4.62E+31	1.41	loud	120789 86416	90020 57150
SDSSJ133045	0.41731	1.16E+30	<1.84E+30	1.4	<9.61E+29	<−0.08	quiet	123743	−7120
[VV96]J232210.8−344757	0.42	3.56172E+30	<1.14E+31	1.4	<3.30E+30	<−0.08	quiet	124214 89905 28339	93507 32260 −2693
SDSSJ111754.31+263416.6	0.422294	2.98E+30	<1.79E+30	1.4	<9.38E+29	<−0.5	quiet	124614	−2209
SDSSJ004222	0.424787	4.36E+30	<2.01E+30	1.4	<1.06E+30	<−0.61	quiet	125048 90822	94417 −5543
SDSSJ143511	0.429945	2.83E+30	<2.00E+30	1.4	<1.05E+30	<−0.43	quiet	125942	−4460
4C−21.35	0.43351	7.60886E+30	1.02E+34	1.4	3.00E+33	2.54	loud	126556	−3714
SDSSJ110406.94+314111.4	0.435718	2.66E+30	<2.08E+30	1.4	<1.10E+30	<−0.38	quiet	123028	607
B0120−28	0.436018	9.41E+29	<1.21E+31	1.4	<6.37E+30	<0.83	quiet	126986	−3190
SDSSJ161649	0.441195	2.73E+30	<1.99E+30	1.4	<1.05E+30	<−0.41	quiet	127870 93929	97498 −2111
SDSSJ080359	0.448706	1.63E+30	<2.06E+30	1.4	<1.09E+30	<−0.17	quiet	123329	91377

Table 2: (continued)

QSO	$z_{\rm em}$	$\log(L_\nu(3000\ ))$ (erg s^{-1} Hz^{-1})	$\log(L_\nu(\rm radio))$ erg s^{-1} Hz^{-1}	ν (GHz)	$\log(L_\nu(5\ \rm GHz))$ erg s^{-1} Hz^{-1}	$\log(\mathcal{R})$	L/Q	$v_{\rm down}$(N v) (km s^{-1})	$v_{\rm up}$(N v) (km s^{-1})
								89718	−553
TON236	0.45	5.96E+30	4.02E+30	1.4	2.14E+30	−0.45	quiet	129360	−285
PG0003+158	0.4509	4.48E+30	4.16E+33	1.4	2.21E+33	2.69	loud	129512	−99
HE0153−4520	0.451	8.95E+30	...	...	...	...	...	129098	2265
SDSSJ100902	0.456524	2.69E+30	3.43E+31	1.4	1.83E+31	0.83	quiet	129595	3236
SDSSJ091029	0.462765	1.59E+30	<2.14E+30	1.4	<1.15E+30	<−0.14	quiet	131491	2342
SDSSJ082024	0.470563	2.18E+30	<2.52E+30	1.4	<1.36E+30	<−0.21	quiet	131924	6279
SDSSJ123304	0.470945	1.51E+30	4.28E+32	1.4	2.30E+32	2.18	loud	132837	4014
SDSSJ161916	0.471598	3.47E+30	<2.57E+30	1.4	<1.38E+30	<−0.4	quiet	132944	4147
SDSSJ092554.70+400414.1	0.471681	1.82E+30	5.28E+31	1.4	2.84E+31	1.19	loud	127222 93992	95635 4164
MRK380	0.475	2.90E+30	<1.44E+31	1.4	<7.75E+30	<0.43	quiet	133500	64406
PG1259+593	0.4778	1.18E+31	<2.64E+30	1.4	<1.42E+30	<−0.92	quiet	133955	7918
HE0226−4110	0.493368	1.65E+31	...	...	...	...	...	136458	11392
SDSSJ155048	0.497235	3.57E+30	<2.62E+30	1.4	<1.43E+30	<−0.4	quiet	137072	9322
HE1159−1338	0.506	2.78E+30	9.65E+31	1.4	5.27E+31	1.28	loud	138452	70327
HS1102+3441	0.508346	1.03E+31	<2.90E+30	1.4	<1.59E+30	<−0.81	quiet	137987	13540
SDSSJ113327	0.524519	2.31E+30	<3.10E+30	1.4	<1.71E+30	<−0.13	quiet	140495	16897
SDSSJ122520	0.535225	3.50E+30	<3.36E+30	1.4	<1.86E+30	<−0.27	quiet	141104 108860	112269 80928
SDSSJ025937.46+003736.3	0.535312	6.66E+30	4.35E+30	1.4	2.41E+30	−0.44	quiet	142958	16836
SDSSJ121850	0.542691	3.29E+30	<3.37E+30	1.4	<1.87E+30	<−0.25	quiet	142233 110120	113518 82275
PKS1136−13	0.556458	2.57E+30	3.37E+34	1.4	1.89E+34	3.87	loud	146106	79588
SDSSJ094331	0.564325	3.94E+30	2.42E+31	1.4	1.36E+31	0.54	quiet	146452	24586
SDSSJ040148	0.570898	5.32E+30	<2.10E+31	1.4	<1.18E+31	<0.35	quiet	148207	23674
PKS0405−123	0.57259	2.95E+31	2.49E+34	1.4	1.40E+34	2.68	loud	148451	23995
SDSSJ124154	0.583471	2.93E+30	<5.89E+30	1.4	<3.33E+30	<0.06	quiet	150006	26047
SDSSJ121430	0.586024	4.28E+30	<4.02E+30	1.4	<2.28E+30	<−0.27	quiet	148584 117231	120556 89894
SDSSJ121640	0.587563	7.49E+30	<3.54E+30	1.4	<2.00E+30	<−0.57	quiet	148803 117477	120800 90159
SDSSJ095000	0.589461	3.96E+30	<3.77E+30	1.4	<2.14E+30	<−0.27	quiet	150853	27170
SDSSJ225738	0.594555	4.85E+30	<2.29E+31	1.4	<1.30E+31	<0.43	quiet	151568	28122
SDSSJ022614.46+001529.7	0.615648	5.62E+30	<3.15E+30	1.4	<1.81E+30	<−0.49	quiet	150979	32022
PG0044+030	0.62326	1.34E+31	1.54E+33	1.4	8.88E+32	1.82	loud	148543 117903	121154 91162
HE0238−1904	0.631	3.33E+31	<2.58E+31	1.4	<1.49E+31	<−0.35	quiet	168855	37462
SDSSJ105945.23+144142.9	0.63171	6.68E+30	<4.57E+30	1.4	<2.64E+30	<−0.4	quiet	156648	34950
SDSSJ111239	0.635972	3.25E+30	<5.64E+30	1.4	<3.26E+30	<0	quiet	153759	35721
3C263	0.646	1.08E+31	3.36E+34	1.4	1.95E+34	3.26	loud	158158	39830
SDSSJ093518	0.649117	6.47E+30	<5.06E+30	1.4	<2.95E+30	<−0.34	quiet	158948	38084
PKS0637−752	0.653	1.58E+31	5.48E+34	1.4	3.19E+34	3.31	loud	159074 129451	132479 79966

Table 2: (continued)

QSO	$z_{\rm em}$	$\log(L_\nu(3000\ ))$ (erg s^{-1} Hz^{-1})	$\log(L_\nu(\rm radio))$ erg s^{-1} Hz^{-1}	ν (GHz)	$\log(L_\nu(5\ \rm GHz))$ erg s^{-1} Hz^{-1}	$\log(\mathcal{R})$	L/Q	$v_{\rm down}$(N v) (km s^{-1})	$v_{\rm up}$(N v) (km s^{-1})
								76402	49407
SDSSJ080908	0.658724	1.06E+31	<4.67E+30	1.4	<2.73E+30	<−0.59	quiet	160196	39796
SDSSJ105958.82+251708.8	0.662779	4.69E+30	<4.73E+30	1.4	<2.77E+30	<−0.23	quiet	160718	73818
								72239	40515
SDSSJ154553.48+093620.5	0.665	1.08E+31	<5.25E+30	1.4	<3.07E+30	<−0.55	quiet	157609	44689
3C57	0.670527	6.19E+30	3.22E+34	1.4	1.89E+34	3.49	loud	161709	41882
PKS0552−640	0.68	5.49E+31	3.61E+33	2.7	3.37E+33	1.79	loud	162534	136359
								133375	84458
								80925	54119
SDSSJ122317	0.682359	5.01E+30	2.41E+31	1.4	1.42E+31	0.45	quiet	161526	135016
								131851	105685
SDSSJ151428.64+361957.9	0.695179	3.96E+30	<5.52E+30	1.4	<3.27E+30	<−0.08	quiet	164798	46179
SDSSJ144511	0.697233	5.26E+30	<5.28E+30	1.4	<3.14E+30	<−0.22	quiet	165051	138774
								135633	46534
SDSSJ113457.62+255527.9	0.709937	8.68E+30	4.10E+32	1.4	2.45E+32	1.45	loud	166603	87557
								85985	54267
SDSSJ124511	0.711698	1.16E+31	1.62E+31	1.4	9.71E+30	−0.08	quiet	...	...
SDSSJ155504	0.714085	3.84E+30	<5.59E+30	1.4	<3.34E+30	<−0.06	quiet	167104	49420
SDSSJ155304	0.722987	1.31E+31	<5.65E+30	1.4	<3.39E+30	<−0.59	quiet	168172	50929
LBQS0107−0232	0.728	1.67E+30	<5.89E+30	1.4	<3.54E+30	<0.33	quiet	168768	51775
SDSSJ091440	0.735438	4.10E+30	<5.38E+30	1.4	<3.25E+30	<−0.1	quiet	168925	55128
SDSSJ100102.55+594414.3	0.747492	2.03E+31	<6.96E+30	1.4	<4.22E+30	<−0.68	quiet	171050	55031
SBS1108+560	0.768267	1.04E+31	<6.85E+30	1.4	<4.19E+30	<−0.39	quiet	173424	58447
SDSSJ143726	0.78226	5.66E+30	<6.38E+30	1.4	<3.92E+30	<−0.16	quiet	174989	60716
SDSSJ234500	0.79005	1.21E+31	<6.81E+30	1.4	<4.20E+30	<−0.46	quiet	171149	144682
								143278	61969
SDSSJ102218	0.790321	1.33E+31	<6.66E+30	1.4	<4.11E+30	<−0.51	quiet	175183	64252
SDSSJ101622.60+470643.3	0.822222	1.00E+31	<6.95E+30	1.4	<4.34E+30	<−0.36	quiet	190132	67062
SDSSJ123426	0.844509	9.71E+30	2.82E+31	1.4	1.77E+31	0.26	quiet	180129	156074
								153178	129020
SBS1122+594	0.85142	1.43E+31	<8.82E+30	1.4	<5.57E+30	<−0.41	quiet	181679	73620
SDSSJ141910	0.874715	1.26E+31	<1.09E+31	1.4	<6.96E+30	<−0.26	quiet	184690	75097
SDSSJ112244.89+575543.0	0.90685	9.47E+30	<8.91E+30	1.4	<5.74E+30	<−0.22	quiet	187819	79852
FBQS0751+2919	0.915726	4.22E+31	2.54E+31	1.4	1.65E+31	−0.41	quiet	185617	84708
PG1407+265	0.94	4.30E+31	2.12E+32	1.4	1.39E+32	0.51	quiet	187926	88169
HB89−0107−025	0.956	9.58E+30	<9.96E+30	1.4	<6.54E+30	<−0.17	quiet	192380	86891
LBQS0107−0235	0.957039	6.44E+30	<9.91E+30	1.4	<6.51E+30	<0	quiet	192473	87036
PG1148+549	0.975979	5.34E+31	1.13E+32	1.4	7.47E+31	0.15	quiet	191232	93174
SDSSJ084349.49+411741.6	0.990788	1.26E+31	<1.11E+31	1.4	<7.36E+30	<−0.23	quiet	195453	91706
CSO0873	1.014695	4.41E+31	<1.22E+31	1.4	<8.16E+30	<−0.73	quiet	155509	128407
								125154	98397
2XMMJ150255.3−415431	1.026	1.62E+30	...	...	...	...	...	193058	171422
								168801	146803
SDSSJ124035	1.046235	9.00E+30	<1.15E+31	1.4	<7.77E+30	<−0.06	quiet	199810	154587

Table 2: (continued)

QSO	$z_{\rm em}$	$\log(L_\nu(3000\ ))$ (erg s^{-1} Hz^{-1})	$\log(L_\nu(\rm radio))$ erg s^{-1} Hz^{-1}	ν (GHz)	$\log(L_\nu(5\ \rm GHz))$ erg s^{-1} Hz^{-1}	$\log(\mathcal{R})$	L/Q	$v_{\rm down}$(N v) (km s^{-1})	$v_{\rm up}$(N v) (km s^{-1})
HE0439−5254	1.053	1.78E+31	...	...	...	...	...	200213	101917
SDSSJ100535	1.0809	2.43E+31	6.15E+31	1.4	4.21E+31	0.24	quiet	202865	103568
SDSSJ120556	1.088576	1.87E+31	1.13E+34	1.4	7.78E+33	2.62	loud	202175 178939	181459 157694
FIRSTJ020930.7−043826	1.128	2.89E+31	7.72E+33	1.4	5.37E+33	2.27	loud	206448	109431
PG1206+459	1.164941	9.50E+31	<1.42E+31	1.4	<9.97E+30	<−0.98	quiet	206537	117161
PG1338+416	1.217076	3.80E+31	<1.60E+31	1.4	<1.14E+31	<−0.52	quiet	210356	119923
HE0435−5304	1.231	2.27E+31	...	...	...	...	...	213658	123309
SDSS−J135726.27+043541.4	1.234529	2.06E+31	<1.81E+31	1.4	<1.30E+31	<−0.2	quiet	213891	121892
HB891038+064	1.27	3.09E+31	5.53E+34	1.4	4.02E+34	3.11	loud	181520 154685	157591 130485
SDSS−J221806.67+005223.6	1.274284	1.39E+31	2.26E+33	1.4	1.65E+33	2.07	loud	...	...
SDSSJ123647	1.287934	2.71E+31	<2.40E+31	1.4	<1.75E+31	<−0.19	quiet	216176 195581	197828 176508
LBQS1435−0134	1.31079	9.34E+31	2.15E+33	1.4	1.58E+33	1.23	loud	216476	130173
PG1522+101	1.328005	7.99E+31	<1.93E+31	1.4	<1.43E+31	<−0.75	quiet	217535	131973
PKS0232−04	1.437368	3.97E+31	3.31E+34	1.4	2.53E+34	2.81	loud	223721	145806
PG1630+377	1.478949	9.21E+31	<2.41E+31	1.4	<1.87E+31	<−0.69	quiet	225940	146730
HS1024+1849	2.84	3.95E+31	<7.73E+31	1.4	<8.13E+31	<0.31	quiet	271021 262619	263471 254243
HE2347−4342	2.885	2.82E+32	...	...	...	...	...	268256	250966
Q0302−003	3.297184	1.03E+32	<6.57E+31	1.4	<7.48E+31	<−0.14	quiet	273854	257848

cal (3000 Å), radio (5 GHz), and X-ray (2 keV) luminosities and the radio-loudness parameter distributions are presented as histograms in Fig. 1. The red shaded regions represent radio-quiet quasars, while the blue shaded regions represent quasars that did not have a radio detection, and so only have an upper limit on L_ν(5 GHz).

3 METHOD FOR SURVEYING ABSORPTION SYSTEMS

We searched the normalized COS spectra for N v systems over the full wavelength coverage up to 10,000 km s^{-1} redward of the peak of the N v emission line. Our criteria for identifying absorption-line systems are as follows.

(1) The stronger member of the N v doublet (1239 Å) is detected at $\geqslant 5\sigma$ confidence using the unresolved feature detection algorithm of Schneider et al. (1993) and Churchill et al. (1999).

(2) The weaker member of the same N v system (1243 Å) is detected at $\geqslant 3\sigma$ confidence (Ganguly et al. 2013).

In addition, the system must satisfy at least one of the following criteria.

(3) The doublets have very similar kinematic profiles, and a physically consistent ratio of equivalent widths.

(4) Lyα, when covered, corroborates the existence of the system.

Although not required, additional lines such as C iv, Si iv, O vi, etc., can be used to help corroborate the existence of the system as well. Such corroboration used in conjunction with criteria (3) and (4) can prove a system may be real even if it has kinetic profiles that greatly differ between the N v 1239 Å and 1243 Å lines in the case of one or both of the profiles being blended. Such criteria can be particularly useful in the case of line-locked systems. Line-locked systems occur when the N v λ1239 transition of one system and the N v λ1243 transition of a second system exist at the same observed wavelength. Line-locked systems can exist in chains, with both transitions of at least one system overlapping with the opposite transition of two other systems. This is another reason criteria (4) is useful to corroborate an absorption system.

4 SURVEY RESULTS

As mentioned in §3, although we conducted a search throughout the entire available spectra to the blue of the quasar redshift and up to 10,000 km s^{-1} to the red of the quasar redshift, we found few N v systems outside of the associated region. Of those systems that we found outside the associated region, most (7 of 10) were high velocity clouds (HVCs) of the Milky Way or at redshifts consistent with known foreground galaxies, making them unlikely to be physically associated with the background quasar[4]. The only system found outside the associated region that can reasonally be assumed to be physically associated with the host quasar is a BAL in the spectra of quasar 2XMM J100420.0+051300, centered at -6351 km s^{-1}, with a width of nearly 4000 km s^{-1}. As mentioned in §1, absorption features with such large widths must be intrinsic. We list the intrinsic systems in our sample in Table 3, along with the emission redshift of the quasar, the absorption redshift of the system, the ejection velocity of the system, the equivalent width of the N v λ1239 Å line, and the error in the equivalent width.

Due to the lack of any intrinsic NAL systems containing N v doublet lines with $|v_{offset}| > 5000$ km s^{-1}, it is found to be unlikely that intrinsic N v NAL systems are found outside of the associated region. Including quasars that do not cover the associated region in their spectra would therefore bias our sample. As such, we created a subsample of quasars using only those quasars for which the associated region is at least partially covered, if not fully covered. All quasars in this subsample have redshifts $z < 0.5$.

In addition, we also required that this subsample contain only Type 1 quasars. Type 2 do not have bright, featureless continuum. They also do not have broad emission lines, which result in lower S/N for the quasar. Type 2 quasar spectra also include a large contribution from starlight in the host galaxy, which make NALs more difficult to detect and bias the sample. Although the Type 2 quasars were searched, no N v absorption was found. It is therefore assumed that the spectra of Type 2 quasars are devoid of N v absorption.

Finally, we also excluded BL Lac objects from the sample, as the continuum we see in their spectra comes from the jet, not the accretion disk. Therefore, any intrinsic systems found would lie between us and the jet, rather than in the host quasar environment, and so would arise in a different environment than the intrinsic N v systems we are surveying. It is of note that the number of BL Lac objects removed from the subsample (14) is nearly equivalent to the number of radio-loud quasars in the subsample (16).

The subsample created using these criteria includes 175 of the original 428 quasars. Figure 2 is the same as Figure 1, but uses only the quasars in this subsample.

4.1 Fraction of Quasars With an Intrinsic System

In this new subsample, we found 58 intrinsic NALs and 1 intrinsic BAL within the spectra of 175 quasars. Of the intrinsic NALs, 39 quasars contained only one intrinsic system, 7 quasars had two intrinsic systems within their spectra, and 2 quasars had three intrinsic systems. There are 48 quasars ($\sim$ 27%) that had at least one intrinsic system. This fraction of quasars containing an intrinsic N v system is consistent with those found in variability studies, such as Narayanan et al. (2004) or Wise et al. (2004), who found intrinsic systems in 25% and 27% of quasars, respectively.

We performed bootstrapping statistical trials to determine if this distribution implied preferred sight lines to the quasars within which intrinsic systems form, such as a given geometry increasing the likelihood of finding an intrinsic system, or if the distribution of intrinsic systems was consistent

[4] Three intervening N v systems were found. The first was in PG0953+414 at $z_{abs} = 0.0681$, $v_{shift} = 43,018$ km s^{-1}. The second was in SDSSJ110406.94+314111.4 at $z_{abs} = 0.2365$, $v_{shift} = 44,447$ km s^{-1}. The third was in 1ES1553+113 at $z_{abs} = 0.1876$, $v_{shift} = 47,834$ km s^{-1}. All other (7 of 10) N v NALs found outside the associated region had redshifts around 0.0001 or less, indicating that they are HVCs.

Table 3. Intrinsic System Properties

QSO	$z_{\rm em}$	$z_{\rm sys}$	v_{ej}[a] (km s^{-1})	$EW_{NV\lambda1239}$ ()	$\sigma EW_{NV\lambda1239}$ ()
(1)	(2)	(3)	(4)	(5)	(6)
NGC 4051	0.00234	0.00111	368	1.99	0.009
NGC 3516	0.00884	0.008	249	1.77	0.009
ESO 267-13	0.0149	0.0139	304	1.23	0.02
NGC-7469	0.0163	0.00981	1926	0.421	0.006
Mrk 1044	0.0165	0.0126	1131	0.2	0.004
NGC 5548	0.0172	0.0154	530	1.42	0.005
UGC 12163	0.0247	0.0242	131	1.4	0.01
MRK 595	0.027	0.0204	1916	0.248	0.009
MRK 595	0.027	0.0254	465	0.0981	0.007
MRK 290	0.0296	0.0287	247	0.243	0.006
MRK 279	0.0305	0.0292	369	0.921	0.02
Mrk 509	0.0344	0.0333	312	0.364	0.002
Mrk 509	0.0344	0.0345	-37	0.523	0.002
2MASX J18324966+5340219	0.039	0.0438	-1380	0.131	0.006
2MASX J18324966+5340219	0.039	0.0444	-1541	0.144	0.007
Mrk 1253	0.049	0.049	-5	0.129	9.0
2MASX J15085291+6814074	0.0586	0.0557	830	0.457	0.01
ESO 265-23	0.0566	0.0554	339	0.0989	0.006
Mrk 1298	0.062	0.0452	4755	0.863	0.02
Mrk 1298	0.062	0.0529	2558	2.88	0.02
Mrk 1298	0.062	0.0584	1007	0.205	0.01
MRK 1513	0.063	0.0576	1524	0.349	0.007
MRK 1513	0.063	0.0631	-29	0.0169	0.003
MR 2251-178	0.064	0.0631	255	0.736	0.006
Ton 951	0.064	0.0646	-166	0.389	0.007
2MASX J14510879+2709272	0.065	0.0642	221	1.86	0.02
Mrk 304	0.0658	0.0579	2221	0.583	0.02
Mrk 478	0.0791	0.0692	2740	0.155	0.009
2XMM J135315.8+634546	0.0882	0.0819	1753	0.905	0.01
2XMM J141348.3+440014	0.0896	0.0895	18	0.441	0.01
LB 1727	0.1	0.1	-126	1.17	0.006
6dFGS gJ031027.9-004951	0.104	0.103	176	0.614	0.002
2MASS J12305003+0115226	0.117	0.106	3008	1.51	0.005
2MASS J12305003+0115226	0.117	0.117	-92	0.336	0.003
2MASS J00362300+4316402	0.12	0.121	-296	2.54	0.02
2MASS J15213967+0337292	0.127	0.125	495	1.1	0.03
2MASX J00481899+3941118	0.134	0.135	-309	0.235	0.003
6dFGS gJ230152.0-550831	0.14	0.139	-315	1.16	0.01
2MASSI J1118302+402553	0.154	0.155	-78	0.238	0.005
2XMM J100420.0+051300	0.16	0.136	-6350	...	...
SDSSJ135625.55+251523.7	0.1640	0.1628	-314	0.1851090869	...
6dFGS gJ015530.0-085704	0.1644	0.1637	-200	0.9575035954	0.0147
2MASS J02121832-0737198	0.174	0.174	-50	0.574	0.01
2E 2135.0-1446	0.2	0.2	-107	0.408	0.005
2E 2135.0-1446	0.2	0.201	242	1.35	0.006
QSO J0012-1022	0.2282	0.2292	235	0.4020647569	0.0232
2MASS J10155924-2748289	0.239	0.242	845	0.288	0.02
Ton 488	0.256	0.255	383	0.813	0.01
6dFGS gJ115758.8-002221	0.26	0.257	881	0.523	0.02
2E 3124	0.264	0.267	-725	0.336	0.02
2MASS J23215113-7026441	0.3	0.301	299	...	...
2MASS J23215113-7026441	0.3	0.301	321	0.148	0.01
2MASS J12072101+2624292	0.322	0.321	299	0.841	0.02
PG 1049-005	0.36	0.342	4033	0.332	0.02
PB 4055	0.383	0.383	116	0.06	0.004
[VV2006] J110313.0+414154	0.403	0.391	2538	0.214	0.02
[VV2006] J110313.0+414154	0.403	0.393	2263	0.406	0.03
[VV2006] J110313.0+414154	0.403	0.4	709	0.545	0.02
QSO J1435+3604	0.429	0.427	306	0.907	0.05

[a] Negative velocity offsets indicate that the absorber is to the blue of the emission redshift.

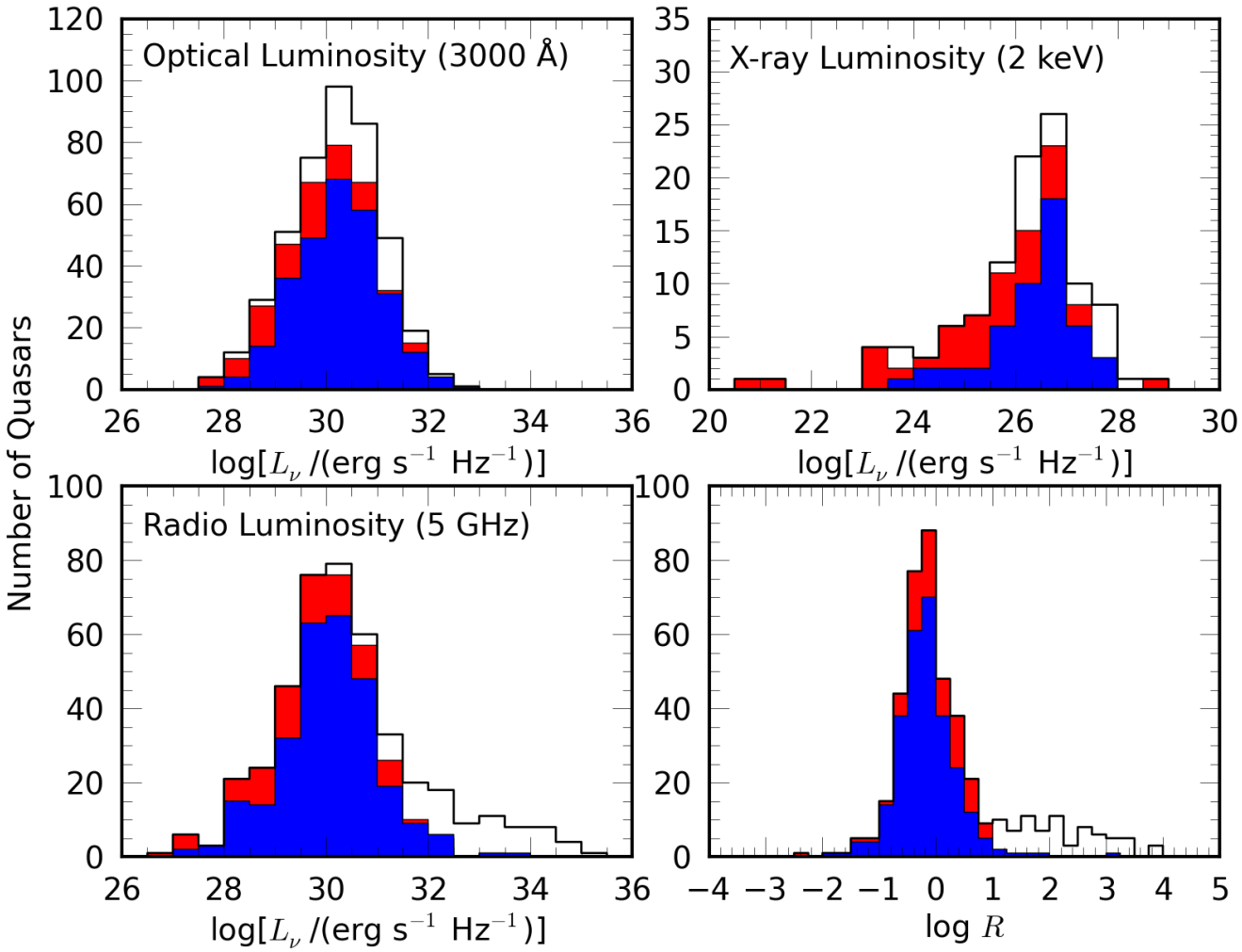

Figure 1. Distribution of optical (3000 Å), radio (5 GHz), and X-ray (2 keV) luminosities, and the radio-loudness parameter for all of the quasars. The unshaded regions represent radio-loud quasars. The red shaded regions represent radio-quiet quasars. The blue shaded regions represent quasars that did not have a radio detection, and so only have an upper limit on L_ν(5 GHz).

with random chance. In these trials, 59 systems were randomly placed within 175 quasars to determine the random distribution (i.e., how many quasars contained one system, how many with 2 systems, etc.). This trial was repeated 100,000 times, and the results were totaled.

When compared with our sample, the results of these trials displayed single systems more often. The average distribution of systems had more quasars with only one intrinsic system, 42.4, than the 39 that were observed in our sample, and the trials resulted in at least 39 quasars with only one system nearly 82% of the time.

The trials also showed fewer quasars with multiple systems. Although they resulted in at least 7 quasars with two systems 59% of the time, the trials resulted in at least 2 quasars with three systems only 17% of the time. As such, we cannot rule out the idea of preferred sight lines for intrinsic N v systems.

These results are at odds with those from those of Culliton et al. (2018a), which found no evidence that at high-redshift, there are preferred sight lines to quasars within which intrinsic absorbers are found. Additionally, although Culliton et al. (2018a) used different methodology to find intrinsic systems, the fraction of quasars with at least one intrinsic N v system in that survey, $11 - 12\%$, is less than half that we found at low redshift. However, if that study had simply used the presence of N v absorption as an indicator of intrinsic absorption as was done in this paper, then that high-redshift sample would have exhibited a *higher* fraction of quasars with intrinsic absorption than was found with the present low-redshift sample. Of the 73 quasars in the high-redshift sample, 26 quasars had at least one associated system with N v absorption present, resulting in a 36% occurrence rate for N v absorption. One possible explanation is that the sample from Culliton et al. (2018a) had a lower equivalent width detection threshold at higher redshift than was allowed in this sample, allowing for weaker systems to be observed. However, few weak N v systems were found. Most of the rest-frame equivalent widths were well above the rest frame equivalent width limit, as well as having similar equivalent widths to those found in this survey. A second possibility for the cause of this change in the rate of occurrence in N v absorption is evolution with redshift, while a third would be that the changes are due to differences in quasar properties. Which of these could be the cause, or in-

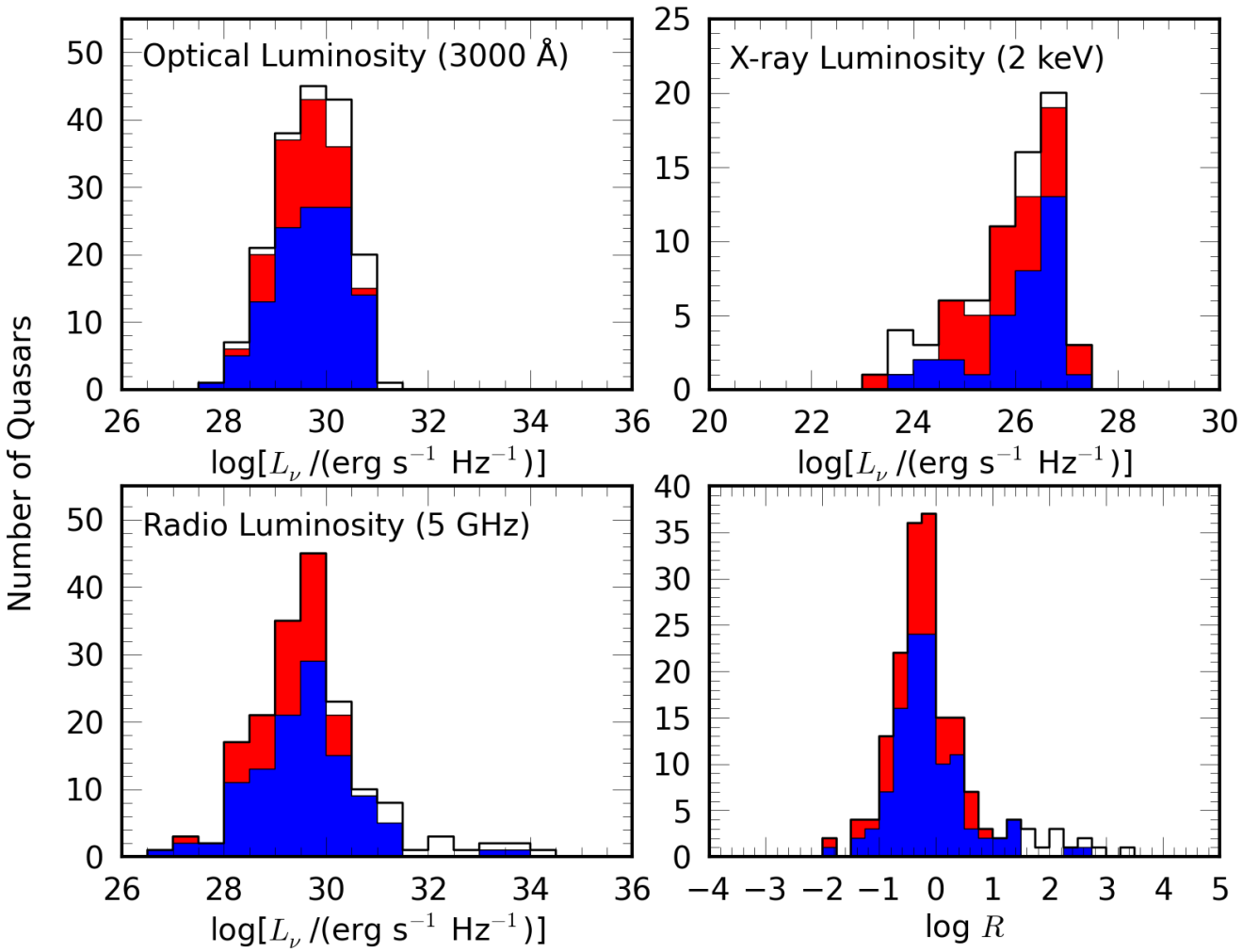

Figure 2. Distribution of optical (3000 Å), radio (5 GHz), and X-ray (2 keV) luminosities, and the radio-loudness parameter for quasars whose spectra at least partically cover the N v assoicated region. These quasars form our subsample. The unshaded regions represent radio-loud quasars. The red shaded regions represent radio-quiet quasars. The blue shaded regions represent quasars that did not have a radio detection, and so only have an upper limit on L_ν(5 GHz).

deed if all three reasons contribute to the change in the rate of occurrence in N v is not yet clear.

4.2 System Properties

Using this survey, we examined the statistical properties of the N 5 absorption systems and their relationships to the quasars hosting them. The systems were described with their N 5 equivalent width and velocity offsets. From the quasars, we considered their optical, X-ray, and radio luminosities, as well as redshift and radio-loudness parameters. For quasars with intrinsic N 5 absorbers, Figure 3 plots the absorber properties against the quasar properties. We then performed statistical tests for each combination of parameters, as seen in in Table 4. Unless otherwise noted, the systems are sorted based on the quasar property given, then divided in half such that the systems originating in quasars with the lowest values of that property are in one group, and those with the highest values in the other. The two groups are then compared using both a Kolmogorov-Smirnov test and an Anderson-Darling test to see if the quasar property affects the given property (equivalent width or velocity offset) of the system at 1% significance. The only statistically significant trend found is that of the velocity offset, sorted by the radio-loudness parameter (seen in the second row, fifth column). As can be seen, the quasars with the largest radio-loudness parameter are unable to accelerate systems to high velocities.

Additionally, though the statistical tests don't conclusively show a difference between equivalent widths at high and low optical luminosities, it should be noted that there are no systems with large equivalent widths within the spectra of quasars with high optical luminosities (seen in the first row, third column). This could imply that quasars with higher luminosities have absorbing material with ionization parameters higher than what optimally allows for systems with strong N 5 lines, resulting in weaker N 5 systems. Another possibility is that is that high luminosity quasars are more efficient at differentially accelerating clouds, causing the cloud to become dispersed as the different regions of the cloud are spread out, weaking the strength of the line at any given velocity offset. Either scenario could lead to smaller

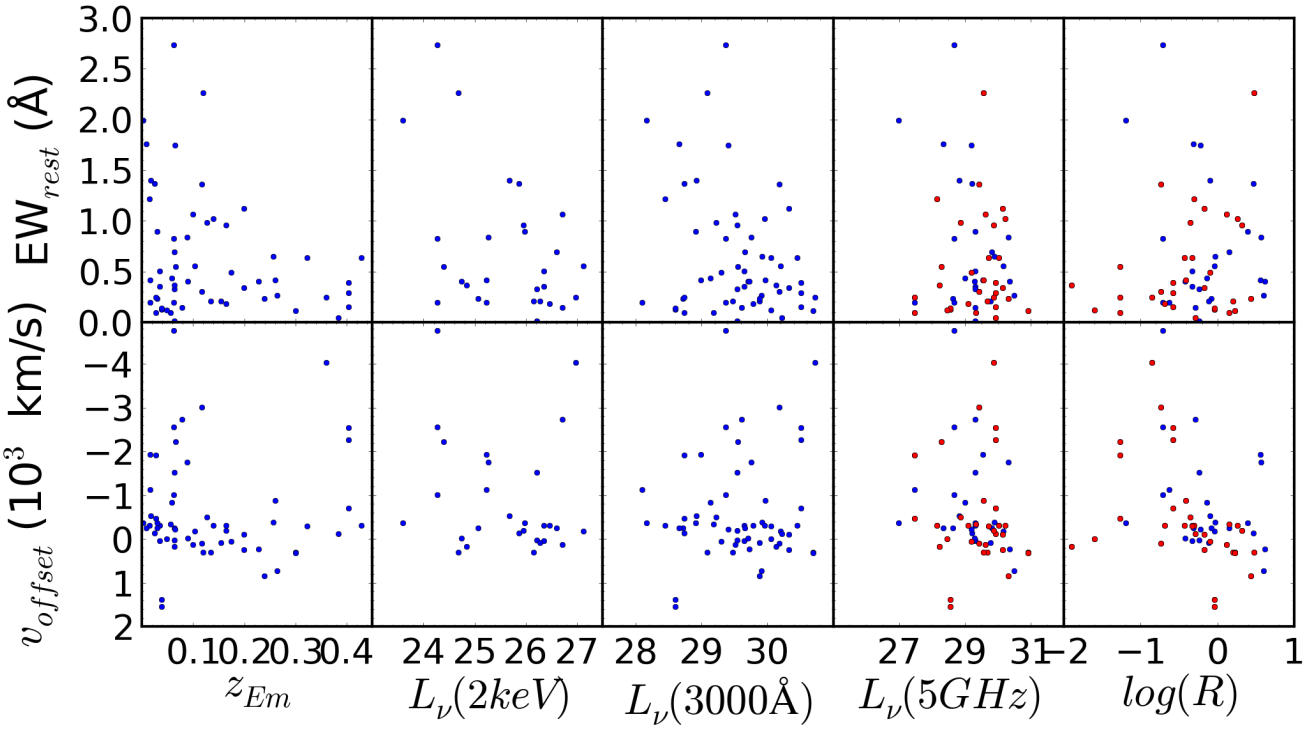

Figure 3. A series of plots comparing the properties of the intrinsic systems (EW and v_{offset}) vs the properties of the host quasars (z_{Em}, L(2 keV), L(3000 Å), L(5 GHz), $\mathcal{R}$). Blue points represent quasars that have a radio detection, while red points represents quasars that did not, and so only have an upper limit for the radio luminosity.

equivalent widths in systems from quasars with higher optical luminosities.

In addition to comparing the properties of quasars that host N 5 systems, it is also useful to compare the properties of quasars that host systems with those that do not in order to determine if N 5 systems have a preference for a specific type of quasar. The statistical results of the Kolmogorov-Smirnov (KS) and Anderson-Darling (AD) tests in which we compare the properties of quasars that host intrinsic N 5 systems vs those without an intrinsic system can be seen in Table 5. Samples with $p < 0.01$ in either test are highlighted in bold. The redshifts of the quasars with systems are significantly different ($p < 0.01$) from those without systems, as those quasars with systems tend to be clustered at lower redshifts than those quasars without systems.

In Figure 4, we compare the properties of quasars that host intrinsic N v systems (red) vs those without an intrinsic system (blue), plotting the properties against each other in order to determine if the quasar properties are related. The five quasar properties plotted on the x-axis and/or the y-axis are redshift, X-ray luminosity, optical luminosity, radio luminosity, and radio-loudness parameter. No obvious trends appear except for those containing radio luminosity and radio-loudness parameter. In those plots, quasars containing an intrinsic system have lower radio luminosities and lower radio-loudness parameters. This trend is highlighted in Figure 5, where we plot the distribution of quasars with respect to radio-loudness parameter. The shaded region represents those quasars with at least one intrinsic system, while the unshaded region represents those without intrinsic systems. The red vertical line represents the criterion for radio-loudness adopted by Kellermann et al. (1989, 1994), $\mathcal{R} \geqslant 10$.

As can be seen, of the 175 quasars in our sample with the associated region at least partially covered, 16 of them are radio-loud. There were 59 total intrinsic N v systems, yet not one of them was found within a radio-loud quasar. If intrinsic systems are equally likely to occur in radio-loud and radio-quiet quasars, the Poisson probability states that there is less than a 0.5% chance for us to find no intrinsic systems within a radio-loud quasar spectrum.

4.3 Sample Comparison

Comparing the results of our sample with other surveys is important in determining similarities and differences, which can hint at underlying properties of intrinsic systems. To this end, we compare the current sample with that of Culliton et al. (2018a). The main difference between the two samples is redshift: Culliton et al. (2018a) has a higher quasar redshift range of 1.4–5, while the redshifts of quasars in our final subsample were all $z < 0.5$. Another difference is that the quasars of the high-redshift sample were more optically luminous than the majority of our sample, without much overlap. Thus, any differences between the two samples could potentially be due to either evolution or to variations within optical luminosity.

The first trend that the high-redshift and low-redshift samples have in common is the relationship between rest-frame equivalent width and radio-loudness parameter (See Figure 6). In both the high-redshift and the low-redshift samples there is a distinct lack of systems with high radio-loudness and equivalent width, regardless of the ion used

Table 4. Statistical Tests of System Properties

Quasar Property[a]	EW[b] ()	v_{offset}[b] (km s^{-1})
High z vs Low z	0.17, 0.78 0.56, 0.63	0.31, 0.087 1.4, 0.084
High $L(3000$) vs Low $L(3000$)	0.29, 0.12 0.44, 0.55	0.25, 0.27 0.48, 0.21
High $L(5\ GHz)$ vs Low $L(5\ GHz)$	0.17, 0.78 0.44, 0.55	0.28, 0.17 0.48, 0.21
High $L(2\ keV)$ vs Low $L(2\ keV)$	0.20, 0.56 0.045, 0.33	0.20, 0.56 0.021, 0.34
High $\mathcal{R}$ vs Low $\mathcal{R}$	0.19, 0.65 0.60, 0.65	**0.42 0.0067** **6.9, 0.00086**
High EW vs Low EW	N/A N/A	0.29, 0.13 1.2, 0.10
High v_{offset} vs Low v_{offset}	0.14, 0.91 0.94, 0.94	N/A N/A
$\lvert v_{offset}\rvert < 600$ km s^{-1} vs $\lvert v_{offset}\rvert > 600$ km s^{-1}	0.31, 0.11 1.2, 0.10	N/A N/A

[a] The quasar property that is used to divide the subsample into two groups. Unless otherwise noted, the systems are sorted based on the quasar property given, then divided in half such that the systems originating in quasars with the lowest values of that property are in one group, and those with the highest values in the other. The two groups are then compared using both the Kolmogorov-Smirnov and Anderson-Darling tests to see if the quasar property affects the given property (equivalent width or velocity offset) of the system.

[b] The quasar property being compared. Results in each cell are in two lines. The first line is the KS-statistic and the p-value of the KS-test. The second line is the Anderson-Darling statistic and the p-value of the Anderson-Darling test. Tests with $p < 0.01$ are in bold.

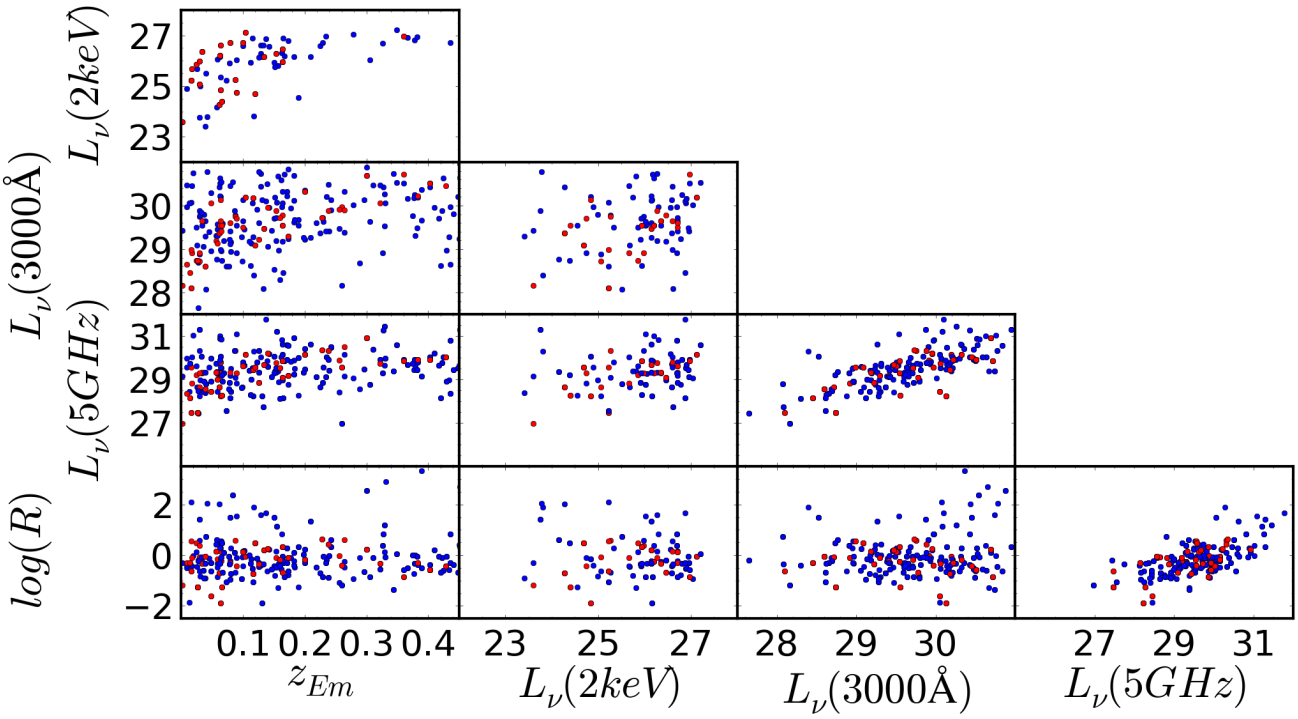

Figure 4. A pair plot of quasar properties (z_{Em}, $L(X-ray)$, $L(optical)$, $L(radio)$, $\mathcal{R}$) in the survey. The blue points represent all quasars, and the red points represent those quasars containing at least one intrinsic system. Quasars with intrinsic systems preferentially have lower luminosities and lower radio-loudness parameters. All quasars within our sample that have an intrinsic NAL present in its spectra are radio-quiet quasars.

[t]

Table 5. Statistical Tests of Quasar Properties

Quasar Property[a]	KS	AD
z	0.25, 0.025	**5.1, 0.0034**
L(3000)	0.28, 0.18	1.1, 0.11
L(5 GHz)	0.19, 0.16	1.7, 0.065
L(2 keV)	0.12, 0.73	0.095, 0.38
$\mathcal{R}$	0.16, 0.30	0.39, 0.23

[a] The quasar property being compared. Results in reported in two cells. The first cell is the KS-statistic and the p-value of the KS-test. The second cell is the Anderson-Darling statistic and the p-value of the Anderson-Darling test. Tests with $p < 0.01$ are in bold.

[h!]

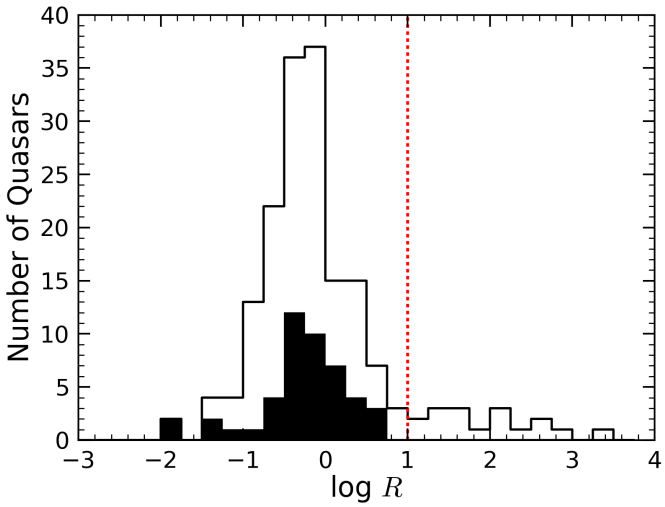

Figure 5. Distribution of the radio-loudness parameter, $\mathcal{R}$, for quasars in our subsample. The black shaded region corresponds to quasars with one or more intrinsic N v systems, while the non-shaded region corresponds to quasars without an intrinsic N v system. The delimiter between radio-loud quasars and radio-quiet quasars is $\mathcal{R} = 10$, denoted in the Figure above with a dashed red vertical line. No radio-loud quasar contains an intrinsic N v system.

to detect the system. Unlike the current low-redshift sample, some systems in the high-redshift sample were found in radio-loud quasars, though aside from one outlier, there are no systems with $EW_{rest} > 0.3$ Å and $\mathcal{R} > 20$. Additionally, the outlier was found using C 4, not N 5. Even though there are some systems from the high-redshift sample that were found in radio-loud quasars using the definition from Kellermann et al. (1989, 1994), there is only one intrinsic N 5 system found above $\mathcal{R} > 30$, and that system had a small rest-frame equivalent width (0.21 Å). Additionally, those N 5 systems found between $\mathcal{R} = 10$ and $\mathcal{R} = 30$ have only upper limits on the radio-loudness parameter. They could potentially reside within radio-quiet quasars. Finally, although it does appear that the systems from the low-redshift sample generally have a greater equivalent width, those systems from the high-redshift sample that do have a relatively large equivalent width are almost all from radio-quiet quasars.

[h!]

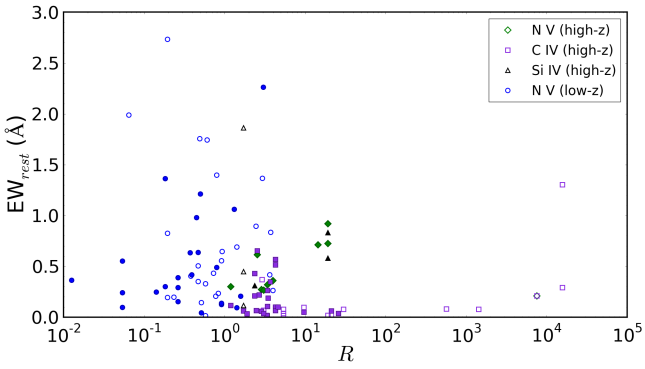

Figure 6. The rest-frame equivalent width, EW_{rest}, vs. the radio-loudness parameter, $\mathcal{R}$ of the current sample and the high-redshift sample from Culliton et al. (2018a). Unfilled symbols represent those quasars that have a defined radio-loudness parameter, while filled symbols are those quasars without radio detections, and so whose radio-loudness parameter is only an upper limit. The N v systems found in this paper are plotted as blue circles. The green diamonds, purple squares, and black triangles represent systems from Culliton et al. (2018a), measuring their equivalent width using N v, C iv, and Si iv, respectively. There appears to be a distinct lack of systems with large $\mathcal{R}$ and large EW_{rest}.

A second similarity between the high-redshift and low-redshift samples is seen in velocity offset vs. optical luminosity (See Figures 7 and 8). Although they are on greatly different scales, both the high-redshift and low-redshift samples show a lack of systems at both high radio-loudness parameter and high velocity offset. Therefore, it appears that quasars with higher ratios of radio to optical luminosities are not able to accelerate systems to velocities as high as those with lower radio-loudness parameters. When we compare velocity offset to optical luminosity instead, a third similarity arises, where the systems with the highest velocity offsets also have the highest optical luminosities. This suggests that increased luminosity allows systems to be accelerated to higher velocities.

One difference between the high-redshift and low-redshift samples is that equivalent width in the low-redshift sample is anti-correlated with optical luminosity, such that the systems with the largest equivalent widths are found in quasars with the lowest luminosities. This trend is not seen in the high-redshift sample. One reason for this could be that the high-redshift sample spans fewer orders of magnitude of optical luminosities ($30 < \log L_\nu(3000\text{ Å}) < 32$) than does the low-redshift sample ($28 < \log L_\nu(3000\text{ Å}) < 31$). A second difference found is that in the high-redshift sample, systems do not have higher equivalent widths within 600 km s^{-1} than they do elsewhere within the associated region. However, the high-redshift sample *does* have higher equivalent widths inside the associated region when compared to those systems outside of it, regardless of the ion used to detect the system (N v, C iv, or Si iv).

[h!]

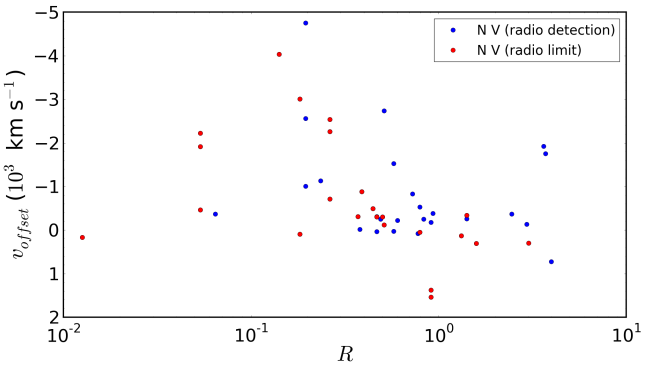

Figure 7. The velocity offset vs. radio-loudness parameter of the current sample. Blue symbols represent those quasars that have a defined radio-loudness parameter, while red symbols are those quasars without radio detections, and so whose radio-loudness parameter is only an upper limit. There appears to be a distinct lack of systems with large $\mathcal{R}$ and v_{offset}.

[h!]

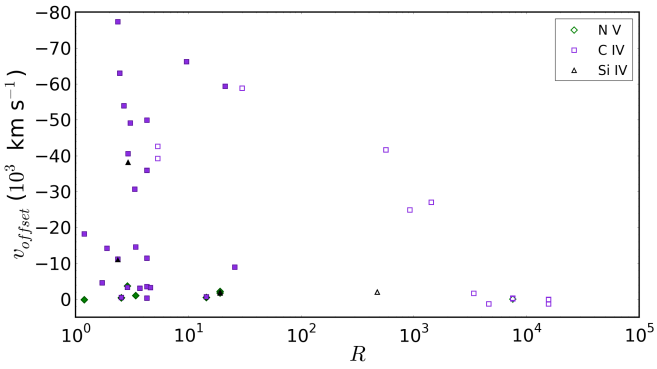

Figure 8. Same as Figure 7, but for the high-redshift VLT sample, with symbols as in Figure 6. Although the ranges over which both axes are covered are much different, just as in Figure 7 there is a distinct lack of systems with large $\mathcal{R}$ and v_{offset}.

5 DISCUSSION

Our primary result from searching the archive of HST/COS observations of quasars/AGN is that none of the 16 radio-loud quasars hosts an intrinsic N V system, whereas their occurrence in radio-quiet quasars is 59 systems in 158 quasars. We compare the distributions of radio-loudness parameter for quasars with and without intrinsic N V systems in Figure 5. The Poisson probability rules out to high confidence ($\geqslant 99.5\%$) that the two distributions are consistent, a significant result. Furthermore, all of the intrinsic N V systems lie near the quasar redshift. There are two ways to interpret this: (1) intrinsic N V systems do not occur in low-redshift radio-loud quasars; or (2) there are no physical differences between where the N V-bearing gas occurs in radio-quiet objects and radio-loud objects, and we just do not see them from our vantage point in the radio-loud subsample.

How could intrinsic N V systems not occurring in low-redshift radio-loud quasars happen? This would point toward a physical difference between radio-loud and radio-quiet quasars in terms of the existence and location of N V-bearing gas. Of course, radio-loud quasars must have *some* N V-bearing gas as evidenced by the presence of the N Vλ1239 emission line. So the lack of N V intrinsic *absorption* points to either a structural/geometric difference or a temporal/evolutionary difference between radio-loud and radio-quiet quasars.

How could we not see the N V-bearing gas that does occur in radio-loud objects? If we suppose that the incidence of N V absorption in radio-quiet quasars is more representative of the number of absorbers along any given sightline to a quasar, then the absence of N V absorbers in radio-loud objects could be an orientation effect. For example, it is possible that our radio-loud quasars preferentially have flat radio spectra, which implies face-on orientations, whereas N V absorption may prefer more edge-on orientations that give rise to steep radio spectra. This would indicate that the incidence of N V absorption is related to some solid angle around the black hole subtended by the N V-bearing gas (i.e., an orientation effect).

Before continuing the discussion, two things are worth acknowledging. First, there is a long history that delves into the potential dichotomy between radio-loud and radio-quiet objects. Second, there is also a long history connecting observationally the presence of $z_{\rm abs} \approx z_{\rm em}$ absorption to the radio-loudness of quasars (Weymann et al. 1979; Foltz et al. 1986; Anderson et al. 1987; Moller & Jakobsen 1987; Aldcroft et al. 1997; Barthel et al. 1997; Richards et al. 1999; Becker et al. 2000; Gregg et al. 2000; Becker et al. 2001; Richards et al. 2001; Richards 2001; Ganguly et al. 2001; Brotherton et al. 2002; Vestergaard 2003; Gregg et al. 2006; Misawa et al. 2007; Miller et al. 2009; DiPompeo et al. 2010; Ganguly et al. 2013; Runnoe et al. 2013). Those studies focused on species (C IV, O VI) that could conceivably arise in the host galaxy or in the environment of the host galaxy. The current study has focused on N V absorption, where there is a higher likelihood that the gas is directly and physically connected with the workings of the quasar central engine.

In thinking about the physical context in which to understand these results, we consider the fundamental parameters that likely define the quasar and its surroundings, namely the black hole, the accretion disk, and the host galaxy. We view the putative "obscuring torus" as an extension of the accretion disk at distances beyond the dust sublimation radius. We take as "key" parameters the following: **black hole** – mass ($M_{\rm bh}$), spin; **accretion disk** – mass accretion rate ($\dot{M}_{\rm acc}$), magnetic field strength ($B_{\rm o}$); and **galaxy** – mass fuelling rate ($\dot{M}_{\rm fuel}$). With these, we have a 5-dimensional space that defines the physical system, or population of systems, plus possible orientation effects to translate these into observations. We posit that these are all independently tunable parameters, without strong physical connections amongst them, but note that certain parameters may constrain others. For example, the accretion rate is capped at some level by the properties of the black hole (e.g., Eddington rate), but the rate itself can be anything below that cap. The accretion rate can potentially also be affected by the magnetic field strength. By definition, the

mass outflow rate, which gives rise to BALs and potentially also the associated/intrinsic absorbers, must be the difference between the mass fueling rate and the mass accretion rate: $\dot{M}_{\rm out} = \dot{M}_{\rm fuel} - \dot{M}_{\rm acc}$.

In the context of these parameters, the primary difference between radio-loud and radio-quiet quasars would likely be that radio-loud quasars must have both a spinning black hole and a strong magnetic field. It is this *combination* that results in the jets and the radio synchrotron emission. Any other combination (e.g., spinning with a weak magnetic field, no spinning with either a strong or weak magnetic field) results in a radio-quiet quasar. What is it about the combination of a strong magnetic field and a spinning black hole that results in not seeing N V in absorption? Probably nothing direct. However, we must consider how other aspects of the system are affected, for example, the radiation field which both ionizes and potentially helps to drive the gas, and also the resulting dynamics.

How is the radiation field changed? We know from observations that radio-loud quasars have harder X-ray spectra (e.g., Miller et al. 2011; Shang et al. 2011). As the spin of the black hole increases, the radius of the inner edge of the accretion disk decreases. With high enough spin rates, the radius of the inner edge of the accretion disk becomes equal to the radius of the black hole's event horizon. As the temperature of the disk is inversely proportional to temperature, allowing the inner edge of the disk to exist at smaller radii allows more energetic photons to be produced. A spectrum that contained more energetic photons would have the effect of ionizing the gas to a higher degree than if those photons were absent. We note, however, that some of the observed hard X-ray emission arises from the polar jets or disk corona. It is not yet clear how the jets would affect the ionization and wind dynamics.

Regardless, we can speculate that the gas launched from the disk is subject to a harder ionizing spectrum. Hence, N 5-bearing gas may be launched from farther out in systems with spinning black holes. Closer in, driving by way of radiation pressure fails because the gas is too ionized. If the N 5-bearing gas is launched from farther out, it might be driven closer to the disk (i.e., if local pressure from the disk does not impart as large of a vertical component). While this would not affect the observation of N 5 in emission, it would require larger inclinations angles to be viewed in *absorption*. In other words, the N 5-bearing gas would subtend a smaller solid angle relative to the black hole. While this may also affect the fraction of radio-quiet quasars with spinning black holes (i.e., those with weak or absent magnetic fields), it would affect other spin/magnetic field combinations that also yield radio-quiet quasars.

Additionally, driving by magnetocentrifugal pressure may also be important. Magnetic fields will also have an affect on the rotational dynamics, in addition to the radial part of the outflow. Without magnetic fields, the wind likely preserves the angular momentum that the outflow had when launched. With the quasar's magnetic field, the wind likely preserves and/or amplifies the angular velocity. This will change the velocity field, and hence the emissivity profile of the disk, and the emission-line region structure. However, it is not clear that this would change from where N V-bearing gas is launched, nor the angle with which it is driven away from the inner disk/black hole.

These orientation effects could be supported by differences seen in low- and high-redshift radio-loud quasars. Although only a few intrinsic N 5 systems were found in high-redshift radio-loud quasars, the fact remains that *some* intrinsic systems were found. If there really is a difference between low- and high-redshift intrinsic system occurrence rate (that is not observational bias), then the answer is likely tied to the black hole mass (statistically higher in high-redshift samples), the mass accretion rate (statistically higher in high-redshift samples), and also possibly the mass fuelling rate (potentially peaking at $z_{\rm em} \sim 2$ as evidenced by the the peak of the quasar number density, and the star-formation rate). Radio-loud objects are still the ones that have spinning black holes with strong magnetic fields, and N 5-bearing gas is still launched at larger radii (in units of $R_{\rm g}$). However, since the accretion rate is larger, so too are the luminosity and the local radiation pressure from where the N 5-bearing gas is launched. Hence, it is conceivable that the gas is launched with a larger vertical component of velocity and N 5 systems subsequently subtend a larger solid angle relative to the inner disk/black hole. A larger solid angle at high-redshift would then imply that the N 5-bearing gas can be observed with a higher incidence in absorption.

In order to determine which parameters were responsible for the distinct lack of N 5 systems within radio-loud quasars, we looked at FIRST radio images of the radio-loud quasars in our sample. Of the 16 radio-loud quasars that cover the N 5 emission line, 10 were covered by FIRST. As shown in Figure 9, 7 of the 10 radio-loud quasars have core-dominated morphologies, with (at most) minor flux contributions from jets. Only three of the FIRST images show far-flung radio-loud lobes, implying an edge-on sightline to the quasar. This means that the majority of radio-loud quasars in our sample have a flat-spectrum, and likely have sightlines that reside close to the poles. This is reinforced by the 14 BL Lac objects removed from the subsample, implying there is a bias in the HST archive to observe face-on, core-dominated radio-loud quasars. We therefore posit that the polar regions of radio-loud quasars are devoid of N 5 systems. Previous studies (Young et al. 1982; Sargent et al. 1988; Ganguly et al. 2001) have found similar results for C 4 systems.

In order to test this hypothesis, we consider a model where there are no intrinsic N V systems within sightlines to core-dominated radio-loud quasars, while for lobe-dominated radio-loud quasars, sightlines are equally as likely as radio-quiet quasars to contain N V-bearing gas. There were 59 systems within 158 radio-quiet quasars, which equates to a rate of occurrence of 0.37 systems per quasar for this high inclination region. Within this model, we would expect to find 1.1 systems within the lobe-dominated quasars. We found zero systems. This result is consistent with our findings from this survey.

This does not, however, answer the question of whether *all* radio-loud quasars are devoid of N V systems, or if only those systems with low inclination angles are devoid of such systems. With 7 core dominated quasars and only 3 lobe dominated quasars, this result could originate from biases in the COS archive for face-on objects due to a selection effect. As only 48 of 158 radio-quiet quasars had at least one N V system, this gives a global covering fraction of $\sim 30\%$. If we assume that radio-loud quasars with large inclina-

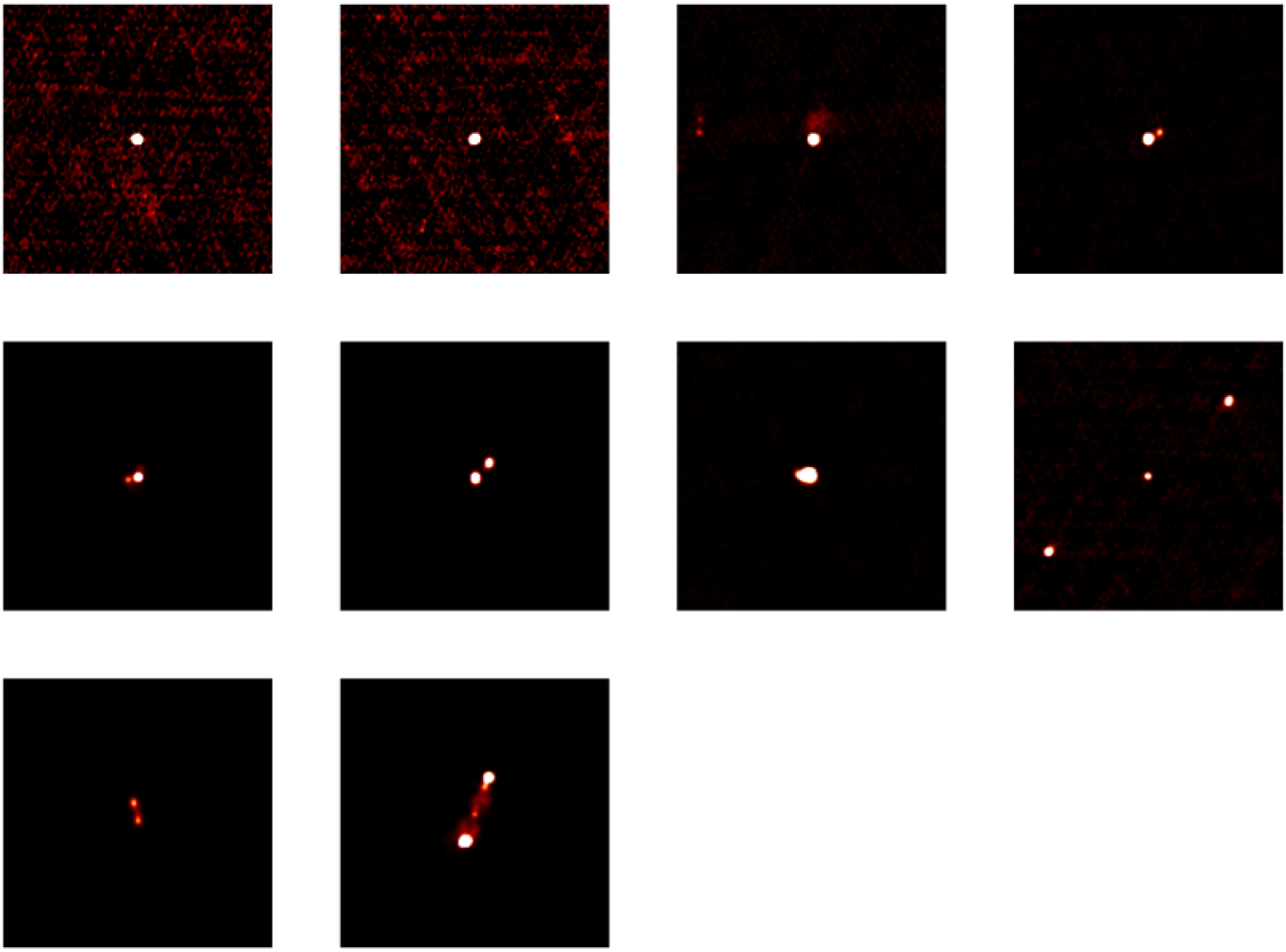

Figure 9. Radio images of the 10 radio-loud quasars that were observed by FIRST. Of those 10 radio-loud quasars, 7 of them exhibit compact radio morphologies, which implies that these quasars have low inclination angles, and are relatively face on.

tion angles have the same covering fraction for N v systems, there is a realistic chance that sightlines towards the lobe-dominated quasars were simply not fortuitous, and a N v cloud did not happen to reside along that sightline, but perhaps exist along other sightlines to the quasar. To determine whether radio-loud quasars are devoid of N v systems, or if the likelihood of finding a N v systems is a function of inclination angle, more observations of steep-spectrum radio-loud quasars are needed. We will attempt to answer this question in Culliton et al. (2018b).

6 SUMMARY

In this survey, we found that 175 of the 428 low-redshift quasars in the HST COS archive were Type 1 quasars with sufficient wavelength coverage that their associated regions are at least partially covered by HST/COS spectra. Within those 175 quasars, we found 59 intrinsic N v systems, 58 NALs and 1 BAL. We described their properties, demographics, and relation of their properties to those of the quasars hosting them. Our findings and conclusions are as follows:

- Within our sample, $\sim 27\%$ of the quasars' spectra contain at least one intrinsic N 5 NAL.
- The equivalent widths of intrinsic N 5 systems are anticorrelated to both optical luminosity and to the absolute value of velocity offset.
- Velocity offset is anticorrelated to the radio-loudness parameter.
- Comparisons with the high-redshift VLT sample from Culliton et al. (2018a) show that both samples have a lack of N 5 systems at large equivalent width and high radio-loudness parameter simultaneously. Similarly, there is a lack of systems with both high velocity offset and high radio-loudness parameter in both samples. Both samples appear to support the idea that larger optical luminosities allow for larger velocity offsets.
- In this low-redshift HST sample, there is a lack of systems with both large equivalent widths and high optical luminosities. This trend is not observed in the high-redshift VLT sample.
- The intrinsic N 5 systems were preferentially discovered within the spectra of radio-quiet quasars. No systems were found in the spectra of radio-loud quasars.
- Core-dominated morphologies were discovered for 7 of

the 10 radio-loud quasars observed by FIRST. Considering there were no intrinsic N 5 systems found within radio-loud quasars, it is possible that such systems are unlikely to be found along the polar axis in radio-loud quasars.

- A follow-up paper (Culliton et al. 2018b) will explore the rate of occurrence of intrinsic N 5 systems at higher inclination angles.

ACKNOWLEDGEMENTS

This work was supported by NSF grant AST-0807993
TM acknowledges support from JSPS KAKENHI Grant Number 15K05020

References

Aldcroft T., Bechtold J., Foltz C., 1997, in Arav N., Shlosman I., Weymann R. J., eds, Astronomical Society of the Pacific Conference Series Vol. 128, Mass Ejection from Active Galactic Nuclei. p. 25
Anderson S. F., Weymann R. J., Foltz C. B., Chaffee Jr. F. H., 1987, AJ, 94, 278
Barlow T. A., Hamann F., Sargent W. L. W., 1997, in N. Arav, I. Shlosman, & R. J. Weymann ed., Astronomical Society of the Pacific Conference Series Vol. 128, Mass Ejection from Active Galactic Nuclei. p. 13 (arXiv:astro-ph/9705048)
Barthel P. D., Tytler D. R., Vestergaard M., 1997, in Arav N., Shlosman I., Weymann R. J., eds, Astronomical Society of the Pacific Conference Series Vol. 128, Mass Ejection from Active Galactic Nuclei. p. 48
Becker R. H., White R. L., Gregg M. D., Brotherton M. S., Laurent-Muehleisen S. A., Arav N., 2000, ApJ, 538, 72
Becker R. H., et al., 2001, ApJS, 135, 227
Brotherton M. S., Croom S. M., De Breuck C., Becker R. H., Gregg M. D., 2002, AJ, 124, 2575
Chiaberge M., Marconi A., 2011, MNRAS, 416, 917
Churchill C. W., Rigby J. R., Charlton J. C., Vogt S. S., 1999, ApJS, 120, 51
Ciotti L., Ostriker J. P., 2007, ApJ, 665, 1038
Culliton C., Charlton J., Eracleous M., Misawa T., 2018a, MNRAS
Culliton C., DeMarcy B., Charlton J., Ganguly R., Eracleous M., Misawa T., 2018b, MNRAS
Danforth C. W., Stocke J. T., Shull J. M., 2010, ApJ, 710, 613
Di Matteo T., Springel V., Hernquist L., 2005, Nature, 433, 604
DiPompeo M. A., Brotherton M. S., Becker R. H., Tran H. D., Gregg M. D., White R. L., Laurent-Muehleisen S. A., 2010, ApJS, 189, 83
Foltz C. B., Weymann R. J., Peterson B. M., Sun L., Malkan M. A., Chaffee Jr. F. H., 1986, ApJ, 307, 504
Ganguly R., Bond N. A., Charlton J. C., Eracleous M., Brandt W. N., Churchill C. W., 2001, ApJ, 549, 133
Ganguly R., et al., 2013, MNRAS, 435, 1233
Granato G. L., De Zotti G., Silva L., Bressan A., Danese L., 2004, ApJ, 600, 580
Green J. C., et al., 2012, ApJ, 744, 60
Gregg M. D., Becker R. H., Brotherton M. S., Laurent-Muehleisen S. A., Lacy M., White R. L., 2000, ApJ, 544, 142
Gregg M. D., Becker R. H., de Vries W., 2006, ApJ, 641, 210
Hogg D. W., 1999, ArXiv Astrophysics e-prints,
Kellermann K. I., Sramek R., Schmidt M., Shaffer D. B., Green R., 1989, AJ, 98, 1195
Kellermann K. I., Sramek R. A., Schmidt M., Green R. F., Shaffer D. B., 1994, AJ, 108, 1163
Miller B. P., Brandt W. N., Gibson R. R., Garmire G. P., Shemmer O., 2009, ApJ, 702, 911
Miller B. P., Brandt W. N., Schneider D. P., Gibson R. R., Steffen A. T., Wu J., 2011, ApJ, 726, 20
Misawa T., Charlton J. C., Eracleous M., Ganguly R., Tytler D., Kirkman D., Suzuki N., Lubin D., 2007, ApJS, 171, 1
Moller P., Jakobsen P., 1987, ApJ, 320, L75
Narayanan D., Hamann F., Barlow T., Burbidge E. M., Cohen R. D., Junkkarinen V., Lyons R., 2004, ApJ, 601, 715
Narayanan A., et al., 2011, ApJ, 730, 15
Osterman S., et al., 2011, Ap&SS, 335, 257
Richards G. T., 2001, ApJS, 133, 53
Richards G. T., York D. G., Yanny B., Kollgaard R. I., Laurent-Muehleisen S. A., vanden Berk D. E., 1999, ApJ, 513, 576
Richards G. T., Laurent-Muehleisen S. A., Becker R. H., York D. G., 2001, ApJ, 547, 635
Runnoe J. C., Ganguly R., Brotherton M. S., DiPompeo M. A., 2013, MNRAS, 433, 1778
Sargent W. L. W., Boksenberg A., Steidel C. C., 1988, ApJS, 68, 539
Scannapieco E., Oh S. P., 2004, ApJ, 608, 62
Schneider D. P., et al., 1993, ApJS, 87, 45
Shang Z., et al., 2011, ApJS, 196, 2
Springel V., Di Matteo T., Hernquist L., 2005, ApJ, 620, L79
Vestergaard M., 2003, ApJ, 599, 116
Weymann R. J., Williams R. E., Peterson B. M., Turnshek D. A., 1979, ApJ, 234, 33
Wise J. H., Eracleous M., Charlton J. C., Ganguly R., 2004, ApJ, 613, 129
Wu J., Charlton J. C., Misawa T., Eracleous M., Ganguly R., 2010, ApJ, 722, 997
Young P., Sargent W. L. W., Boksenberg A., 1982, ApJS, 48, 455